Aspects of Response in Topological Materials to Broken Time Reversal Symmetry

By
TAYYABA AFTAB

DEPARTMENT OF PHYSICS
QUAID-I-AZAM UIVERSITY
ISLAMABAD
2020

Aspects of Response in Topological Materials to Broken Time Reversal Symmetry

The thesis is submitted in partial fulfillment of the requirements for the award of degree of

DOCTOR OF PHILOSOPHY
IN
PHYSICS

By
TAYYABA AFTAB

DEPARTMENT OF PHYSICS
QUAID-I-AZAM UNIVERSITY
ISLAMABAD
2020

Author's Declaration

I Tayyaba Aftab hereby state that my Ph.D thesis titled **Aspects of Response in Topological Materials to Broken Time Reversal Symmetry** is my own work and has not been submitted previously by me for taking any degree from Quaid-i-Azam University, Islamabad or any where else in the country/world.

Any time if my statement is found to be incorrect even after my graduation the university has the right to withdraw my Ph.D. degree.

Tayyaba

Tayyaba Aftab
August 26, 2020

Plagiarism Undertaking

I solemnly declare that research work presented in this thesis titled **Aspects of Response in Topological Materials to Broken Time Reversal Symmetry** is solely my research work with no significant contribution from any other person. Small contribution/help wherever taken has been duly acknowledged and the complete thesis has been written by me.

I understand the zero tolerance policy of the HEC and Quaid-i-Azam University Islamabad towards plagiarism. Therefore I as an Author of the above titled thesis declare that no portion of my thesis has been plagiarized and any material used as reference is properly referred/cited.

I undertake that if I am guilty of any formal plagiarism in the above titled thesis even after award of Ph.D degree, the university reserve the right to withdraw/revoke my Ph.D degree and that HEC and the university has the right to publish my name on the HEC/University website on which names of students are placed who submitted plagiarized thesis.

Tayyaba

Student/Author Signature
Name: Tayyaba Aftab

Certificate of Approval

This is to certify that the research work presented in this thesis, entitled "**Aspects of Response in Topological Materials to Broken Time Reversal Symmetry**" was conducted by Ms. Tayyaba Aftab under the supervision of Prof. Dr. Kashif Sabeeh.

No part of this thesis has been submitted anywhere else for any other degree. This thesis is submitted to the Department of Physics, Quaid-i-Azam University Islamabad, Pakistan in partial fulfillment of the requirements for the degree of Doctor of Philosophy in Physics, Department of Physics Quaid-i-Azam University Islamabad.

Student Name: **Ms. Tayyaba Aftab** Signature: Tayyaba

Examination Committee:

a) Dr. Shafqat Hussain Shah Signature:
Principal Scientist
Computational materials Design Group
PINSTECH, P.O. Nilore, Islamabad.

b) Dr. Arshad Saleem Bhatti Signature: Arshad Saleem
(Dean Natural Sciences)
Department of Physics
COMSATS, Institute of Information Technology,
ChakShahzad, Park Road, Islamabad.

c) Prof. Dr. Nawazish Ali Khan Signature: 26-5-2021
Chairman
Department of Physics
QAU, Islamabad

Prof. Dr. Kashif Sabeeh Signature:
Supervisor,

Chairman Signature: 26-5-2021

Declaration

This is to certify that the work presented in the thesis titled **Aspects of Response in Topological Materials to Broken Time Reversal Symmetry** was carried out by **Ms. Tayyaba Aftab** under our supervision and is accepted in its present form by the Department of Physics, Quaid-i-Azam University, Islamabad as satisfying the dissertation requirement of the degree of

DOCTOR OF PHILOSOPHY IN PHYSICS

Supervisor

Prof. Dr. Kashif Sabeeh
Department of Physics
Quaid-i-Azam University
Islamabad, Pakistan.

Submitted through

Prof. Dr. Nawazish Ali Khan
Chairman
Department of Physics
Quaid-i-Azam University
Islamabad, Pakistan.

Dedicated to

Ammi, Agha G and Zain

Acknowledgement

All the acclamations and glories are for ALMIGHTY ALLAH, the Creator of all things and only worthy to be worshiped. Countless salaams for the last Holy Prophet MUHAMMAD (PEACE BE UPON HIM), whose teaching has guided us through darkness.

I would like to thank ALLAH for HIS divine help, love and care. For selecting me to be amongst those lucky people who have countless blessings.

My immense gratitude goes to my honorable supervisor **Prof. Dr. Kashif Sabeeh** for his expert guidance, ideas, inspiration, motivation and keen interest in my research work and throughout my university life. His way to teach and guide was undoubtedly great. His role has been very important throughout my university life. Furthermore I thank to **Prof. Dr. Nawazish Ali Khan** (Chairman Department of Physics) for providing the facilities for research work. Who has supported me through thick and thin in my academic career. I thank to Prof. Dr. Zafar Ilyas and Dr. Bushra Iqbal for their support and inspiration which played vital role in the making of this thesis.

I would like to mention my family who has supported me by all possible means. My parents who have been loving me unconditionally no matter what. Who always prayed for me. My husband, **Dr.Muhammad Nasir** who was not only supportive but guided me in many ways. My sisters,(**Samra, Humera and Sidra**) and brother, **Agha Yasir** have always been very supportive.

I would like to thanks my dearest son, **Zain Ali** for the smiles, kisses and hugs, which make me energetic everyday after a tiring day. Who is a miracle of my life. Someone who brings motivation to live and survive.

I thank to some special friends who played major role in my life at qau. Dr. Kulsoom Rahim and Dr. Muhammad Usman are the best people I ever met. I extend my thanks to my friends Dr. Ambreen Uzair, Dr. Gul-e-Ali, Sunia Hassan, Atif Masood, Abdul Rehman, Rabia Nazish, Aruza Naeem, Maryam Hassan and Yusra Anwar.

I am also thankful to the staff of the Department of Physics, Quaid-i-Azam University, Islamabad, especially Mr. Khadam Hussain (late), Mr. Dur-e-Iman, Mr. Muhammad Sadiq, Mr. Ijaz Ahmad, Mr. Ifrahim Siddique, Mr. Akhlaq Ahmad, Mr. Faisal, Mr. Muhammad Kamran and Mr. Abdul Gaffar for their continuous cooperation all the time during my research.

Tayyaba Aftab

List of Publications

This thesis contains the following research articles published in the international journals:

1. Valleytronics and phase transition in silicene, **Tayyaba Aftab**, *Physics Letters A*, **381**, 10 (2017).
2. Anisotropic magnetic response of Weyl semimetals in a topological insulator multilayer, **Tayyaba Aftab**, Kashif Sabeeh, *Journal of Applied Physics* **127**, 163905 (2020).
3. Far from equilibrium Dynamical Response in Photoinduced Semi-Dirac Materials, **Tayyaba Aftab**, Kashif Sabeeh, *in preparation*.

Abstract

In this thesis, response of some representative topological materials is studied when Time Reversal Symmetry (TRS) is broken. Topological materials include topological insulators, topological semimetals and topological superconductors. We study the topological response in silicene and it is shown to be encoded in terms of Berry curvature, magnetic moment, Hall conductivity and polarization. It is found that when TRS is broken via external magnetic field the topological response of silicene is valley dependent and leads to valleytronics. Magnetic response of Weyl semimetals is investigated when TRS is broken in the presence of external magnetic field tilted at an angle θ. Magnetic susceptibility is found to be anisotropic which can be employed to distinguish orbital, spin-orbital and spin response. In addition to the above mentioned near equilibrium responses of Dirac materials, far from equilibrium dynamics of Dirac materials is studied through quantum quenching. The persistant Hall current is shown to exist for late times in semi-Dirac materials even in the presence of TRS; which is contrary to what one expects for equilibrium states.

Contents

List of Figures

Chapter 1

Introduction

Topology is a well established branch of mathematics which has found numerous applications in condensed matter physics. There has been a great deal of recent interest in the study of topological phases in materials. A remarkable aspect of topological phases is their robust behavior against certain deformations in the Hamiltonian. The history of topological phases in condensed matter systems started with the discovery of the quantization of Hall conductivity[1] in 2D electron gas in the presence of a strong magnetic field. Extreme quantization of Hall conductivity was found to have topological origins. The quantization of Hall conductivity was a ground breaking discovery and this laid the foundation of topological phases in condensed matter[2, 3, 4, 5, 6, 7, 8] in the presence of strong magnetic field. The appearane of non- zero Hall conductivity was attributed to breaking of Time Reversal Symmetry (TRS) in a 2D electron gas but it was shown later by Haldane that one can have quantum Hall effect even in the absence of TRS.

Several of the earlier topological phases were observed in two-dimensional (2D) materials. The field of 2D materials received a great boost by the discovery of graphene; a single sheet of graphite. Graphene at half filling is a semimetal with low energy excitations that exhibit relativistic dispersion. These excitations are known as massless Dirac fermions. After the discovery of graphene, Topological Insulators (TI), a new class of materials with topological phases were discovered. TIs are insulating in the bulk and have conducting boundary modes[9, 10]. They are stable to deformations due to bulk energy gap which is characterized by a topological invariant[10, 11, 12] similar to Chern number. Both 2D ($HgTe/CdTe$) and 3D ($Bi_{1-x}Sb_x, Bi_2Se_3, Bi_2Te_3$ and Sb_2Te_3) TIs have been studied extensively[13, 14, 15, 16, 17].

Unlike TI, Dirac semimetals have no bulk gap and are characterized by topological invariants as well. These materials are known as topological semimetals[18, 19, 20, 21, 22]. They are time reversal and spatial inversion symmetric. When either symmetry is broken four fold degeneracy shifts to double degenerate points known as Weyl nodes and such point nodal materials are called Weyl semimetals.

The Dirac-like dispersion puts all these materials into a single class known as Dirac materials, which are of special interest because they are known to host response that is of topological origin. The low energy effective Hamiltonian of Dirac materials is Dirac-like [20, 21, 22, 23, 24]. They include topological insulators, graphene, topological semimetals and topological superconductors. These apparaently different materials share common features [25]. Many features and aspects of Dirac materials have been studied extensively like magnetotransport[26], Floquet response[27], Strain effects[28], valleytronics[29] and quantum transport[30].

Our aim, in this thesis is to study the following two main problems: one is to study the near equilibrium response of Dirac materials when TRS is broken. This is done within the linear response theory. Whether a system breaks TRS or not has profound effect on its properties. In a classical context, time reversal operation $t \to -t$ can be treated as reversal of motion. In quantum mechanics it is implemented by the time reversal operator which is an antiunitary operator $T = UK$ where U is a unitary operator and K is complex conjugate operator.

In this thesis, work presented in Chapter 2 and 3 was carried out in the presence of an applied magnetic field which explicitly breaks TRS. In Chapter 4, TRS plays a more subtle role. A careful study of non-equilibrium dynamics in the presence and absence of TRS breaking terms is presented in this chapter.

1.1 Thesis overview

The response that we study is encoded in terms of Berry curvature, magnetic moment, Hall conductivities (spin and valley) and magnetic susceptibility. Explicit breaking of TRS is carried out by an applied magnetic field. To examplify this, the first material we choose is silicene and we investigate the spin and valley transport in this material. This is presented in Chapter 2. As compared to graphene, silicene is a better potential candidate to study spin as well as valley related features due to relatively stronger SOC. Silicene is a monolayer of silicon atoms that forms a two dimensional honeycomb lattice. Due to its unique properties, silicene has attracted much attention both theoretically and experimentally [31, 32, 33, 34, 35]. Though fabrication and synthesis of silicene was a challenge because of issues related to its stability in air but researchers fabricated it using a growth transfer process and made transistors that work at room temperature. This approach is proposed to be effective for other two dimensional materials like germanene and phosphorene[36]. Recently surface studies of silicene have been carried out using low temperature atomic force microscopy[37]. Like graphene there is Dirac like electron dispersion at K points of the Brillouin zone in silicene as well. This and many other similarities are observed because their constituents are atoms that belong to the same column in the periodic table. But silicene possesses stronger SOC than graphene, which can be increased under strain. Silicene is thus a better system for studying the spin and valley physics not prominent in graphene due to its smaller SOC. Further, the band gap in silicene is tunable with external electric field. The sites on the sub-lattices are in different vertical planes with separation causing silicene to be buckled. When electric field perpendicular to the plane is applied, then on site potential difference arises[38, 39]. Valley-spin locking, non-zero Berry curvature and quantum phase transition from Hall insulator to band insulator is observed in silicene when both TRS and inversion symmetries are broken. Valley contrasting feature appears due to breaking of TRS[40]. Silicene has been extensively studied using DFT and first principle calculations. DFT studies of adsorption of toxic gases on silicene and its possible use as a gas sensor[41], in anticancer drugs[42], uric acid adsorption[43], DNA sequencing[44] and quantum dots of silicene in nanomedical diagnostics[45] have been performed.

Next we study the magnetic response of Weyl semimetals. This is presented in Chapter 3. Weyl semimetals from the class of topological semimetals are chosen to study the magnetic sus-

ceptibility in the presence of an external tilted magnetic field. Weyl semimetals are anisotropic in nature and they have all three types of magnetic susceptibilities: orbital, spin and spin-orbital susceptibility, when placed in a tilted magnetic field. The three types of susceptibilities are distinguished by the orientation of the applied magnetic field[46]. Weyl semimetals are topological materials which hosts Weyl fermions. They have gapless bulk and non degenerate valence and conduction bands touching at certain points and are known as nodal Weyl semimetals. They are considered as three dimensional analogue of graphene. They were initially theoretically proposed in pyrochlore iridates [47], $HgCr_2Se_4$ [48] and multilayer of topological insulator and normal insulator[49]. There are other types of semimetals in which degeneracy occurs on a reciprocal space line and such materials are called line node semimetals. By taking thin films of alternating layers of TI and normal insulator (NI) in the presence of magnetic impurities both types of semimetals can be realized[49, 50] depending on the direction of magnetic moments. A minimal model for these topological semimetals, that is employed in this thesis, is a topological insulator multilayer that was proposed by Burkov and Balents[51]. It consists of alternating thin layers of Topological Insulators (TI) and Normal Insulators (NI) in the presence of magnetic impurities. These thin layers are coupled by tunneling across the NI and between top and bottom of TI, Fig. 3.1. The quasi particles in this system are Dirac fermions and their mass is tuned by the thickness of the thin films. Existence of nodal semmetals has been verified in a number of experiments on different materials[47, 49, 50, 52, 53, 54, 55, 56].
The second problem we address is to investigate aspects of far from equilibrium dynamics in Dirac materials presented in chapter 4. To access this non-equilibrium dynamics, we consider quenching the system. This requires preparing a quantum mechanical system in the initial eigen state of a given Hamiltonian; At a later time we abruptly change a parameter in the Hamiltonian driving the system into a non-equilibrium phase. We then allow the system to evolve to study its dynamical response. These properties have no equilibrium analog and to study these far from equlilibrium properties quenching a parameter is a useful tool[57, 58, 59]. This technique has been used to study response of fermions to local quenches[60], investigation of Berry curvature and topological invariants in one and two dimensional systems [61], bulk and edge currents in frustrated bosonic and normal fermionic systems[62] and Bose-Einstein condensates [63]. Photoinduced far from equilibrium effects have been studied in graphene and[64] topological insulators[65] using quantum quenching. Floquet Hamiltonian and systems are discussed using quenching of parameters in Chern insulators[66] and topological insulators [67, 68]. We specifically discuss far from equilibrium physics in semi-Dirac materials which is accessed through quantum quenching the system. Physically this is achieved by exposing the material to linearly polarized light. Non equilibrium response is manifested in persistant Hall current that survives for long times even when instantaneous TRS is not broken; this has no equilibrium counterpart[69].

The final chapter 5 is summary of the thesis.

Chapter 2

Response of Silicene to Broken Time Reversal Symmetry

2.1 Introduction

The topological response of materials is studied in terms of topological invariants. These topological invariants can be related to Berry curvature, magnetic moment and Hall conductivity. In this chapter, we study the topological response of silicene. Over the past few years, it has been found that the Berry curvature has a major role in the physical properties of materials. It is an intrinsic property of bands as it depends on the wave function. It is nonzero in crystals with broken inversion or time-reversal symmetry[70].

In materials with valleys in the band structure, a valley degree of freedom similar to but different from spin can appear. This has given birth to the field of valleytronics [71, 72]. A seminal work in this regard was the study of valley contrasting peoperties of graphene. In graphene, valley polarization has been proposed to be detected when inversion symmetry is broken. Each valley is characterized by opposite Hall transport i.e. the carriers flow to different transverse edges when electric field is applied perpendicular to the system[71]. In silicene it has been discussed with electric field applied to the system[73] and in the presence of magnetic field[74]. It was observed that graphene[71] and Transition Metal Dichalcogenides (TMD)[75] show valley contrasting behavior in the presence of substrate potential. For TMD there is an extra contribution from spin splitting and that leads to asymmetric Landau levels[76]. Valley degree of freedom can be controlled using circularly polarized light which allows the possibility of the use of valley excitons for applications in quantum information and ultrafast devices. Valleytronics is an emergent field which deals with valley based electronic applications and it needs valley degree of freedom to be treated separately to manipulate the contrasting physics of two valleys effectively[77, 78, 79, 80, 81]. With optical light, it opens up the possibility of coherent manipulation of the valley polarization in TMD[82, 83, 84]. For graphene valley-dependent physics, generation and experimental control of valley polarization, have been explored[85, 86, 87, 88]. Creating valley polarization is rather less straightforward but has been shown for $AlAs$, Bismuth, graphene and MoS_2[89].

Silicene in the presence of electric and magnetic fields has been shown to exhibit Hall effect[90]. In the presence of exchange field with intrinsic and extrinsic Rashba coupling, Chern insulating states with non zero Chern numbers have been shown to appear in silicene[91]. It has been shown that the combination of electric and magnetic fields with intrinsic SOC lead to topological phase transition, without taking pseudospin degree of freedom into account[74]. It has been seen that a phase transition occurs from a topologically trivial to a band insulating state and further to a semi metallic state in an inhomogeneous electric field applied perpendicular to silicene[73, 92]. Topological response of silicene in terms of Berry curvature and magnetic moments is discussed in Sec.2.3.1 and Sec.2.3.2 when silicene is placed in electric and magnetic fields in proximity with a magnetic material. For the valleytronics, valley polarization is important; in the context of silicene this is discussed in Sec.2.3.3. We show that an interplay of uniform electric field and SOC can be used to tune silicene from a semimetallic state to a topological insulating state which is discussed in Sec.2.3.4.

2.2 Formulation

In this part of the chapter silicene and its topological response will be discussed in detail. Silicene is taken to lie in the xy-plane in proximity with a magnetic material, h being the exchange field due to this proximity effect. The sheet is exposed to external electric and magnetic fields. The effective Hamiltonian is given[93, 94, 95] as

$$H^{\alpha}_{\sigma_z} = \hbar v(\alpha k_x \tau_x + k_y \tau_y) - \Delta_{so}\alpha\sigma_z\tau_z + \Delta_z\tau_z + h\sigma_z \tag{2.1}$$

The first term is graphene like for Dirac fermions in buckled silicene with $v = 5\times 10^5 m/s$, σ_z is the spin index and $\alpha = \pm 1$ is a symbol used to indicate valley K and K', the second term is SOC term as described by Kane and Mele[11], where Δ_{so} is the spin orbit coupling gap induced by this term; taken to be $7.9meV$[96]. From density functional theory calculations $\Delta_{so} = 1.55meV$[97],[98],[99] and tight binding calculations $\Delta_{so} = 7.9meV$[99]. The next term is associated with electric field with $\Delta_z = a_0 E_z$, where E_z is an electric field which is applied perpendicular to the silicene sheet and $a_0 = 0.23A^0$. h is an exchange field in the last term due to proximity effect, $h = 1.1meV$, $h = 9meV$[95]. In this chapter, τ_i are the Pauli matrices acting in the sublattice space which differentiate **A** and **B** sub-lattices. Valley physics arises because of the inversion symmetry breaking and here electric field plays the role of the symmetry breaking field. In the presence of perpendicular magnetic field B, the vector potential A is taken to be $(0, Bx, 0)$ and this term alongwith last term in Eq.(2.1) explicitly breaks TRS of the system

The Hamiltonian defined in Eq.(2.1) after Peierls substitution becomes:

$$H^{\alpha}_{\sigma_z} = \begin{pmatrix} h\sigma_z - \Delta_{so}\alpha\sigma_z + \Delta_z & v_f[\alpha(p_x + eA_x) - i(p_y + eA_y) \\ v_f[\alpha(p_x + eA_x) + i(p_y + eA_y) & h\sigma_z + \Delta_{so}\alpha\sigma_z - \Delta_z \end{pmatrix}. \tag{2.2}$$

Taking $\boldsymbol{\pi} = \boldsymbol{p} + e\boldsymbol{A}$. Let $\Delta_B a = \pi_x - i\pi_y$, $\Delta_B a^\dagger = \pi_x + i\pi_y$ be the annihilation and creation operators respectively, where $\Delta_B = \sqrt{2\hbar e B}$

The energy spectrum after diagonalizing the Hamiltonian in Eq.(2.2) is:

$$E^{\alpha}_{\sigma_z}(n, s) = h\sigma_z + s\sqrt{n\Delta_B^2 + (\Delta_{so}\sigma_z - \Delta_z\alpha)^2} \tag{2.3}$$

where $s = \pm$ are the electron/hole bands and n is an integer indexing the Landau levels.

The zero mode energy is:

$$E^{\alpha}_{\sigma_z}(0, s) = h\sigma_z + s(\Delta_{so}\sigma_z - \Delta_z\alpha). \tag{2.4}$$

The interplay between Δ_{so} and Δ_z play a major role in tuning the energy. The zero modes show a phase transition from TI to BI for zero exchange field due to band inversion[96] but with non-zero exchange field degeneracy points are shifted .

The corresponding wave functions are calculated to be:

$$\Psi^{\alpha}_{\sigma_z}(n) = \begin{pmatrix} t_1\Phi_{n-1} \\ t_2\Phi_n \end{pmatrix} \tag{2.5}$$

$$\Psi^{\alpha}_{\sigma_z}(n') = \begin{pmatrix} t_1\Phi_{n'} \\ t_2\Phi_{n'-1} \end{pmatrix} \tag{2.6}$$

where Φ_n is Hermite polynomial, $t_1 = \sin(\frac{\theta_n}{2})$, $t_2 = \cos(\frac{\theta_n}{2})$ with $\theta_n = \tan^{-1}(\frac{\sqrt{n}\Delta_B}{\Delta_{so}\sigma_z - \Delta_z\alpha})$.

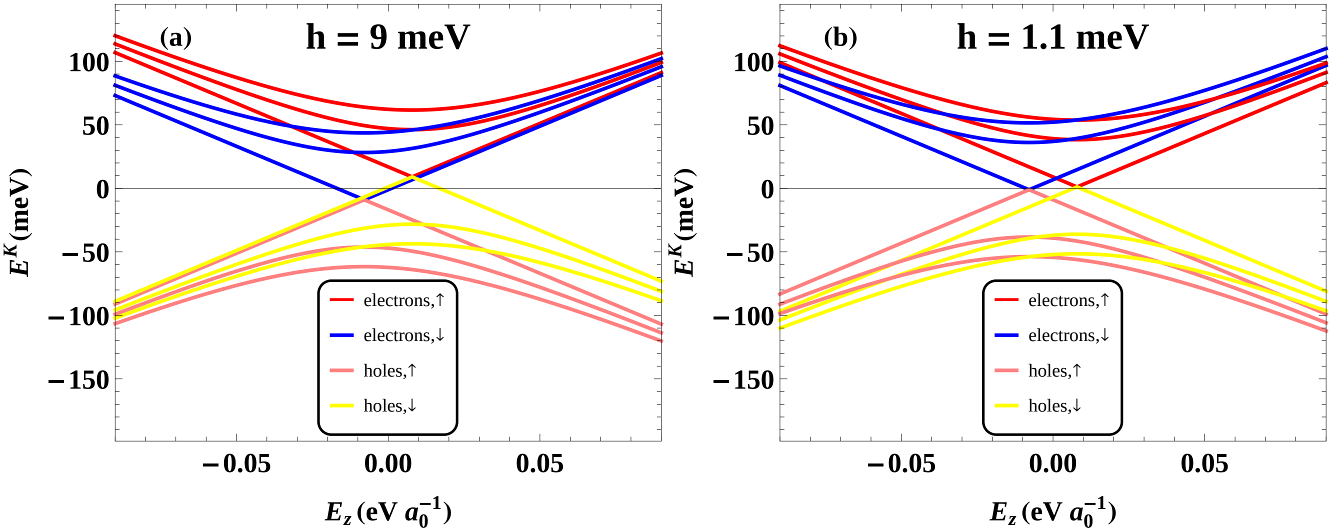

Figure 2.1: Energy dispersion for K valley, varying with perpendicular electric field. $\Delta_{so} = 7.9meV$, $B = 4.1T$, $a_0 = 0.23A^0$.

With exchange field of $9meV$ dispersion relation exhibits shift in Dirac point from $0eV$ to $0.01eV$ as depicted in Figs.2.1(a), 2.2(a) and with exchange field of $1.1meV$ dispersion relation exhibits shift in Dirac point from $0eV$ to $0.01eV$ as depicted in Figs.2.1(b), 2.2(b). Interestingly Dirac point for spin up of both valleys is shifted to the conduction band and spin down to the valence band. Thus polarization of spins is possible, which is an important step towards spintronics. Exchange field is coupled to spin that is the reason of its role in spin dependent devices. In the following sections we study the response of silicene to perpendicular magnetic field.

2.3 Response of Silicene to magnetic field

Some topological responses of silicene are discussed below.

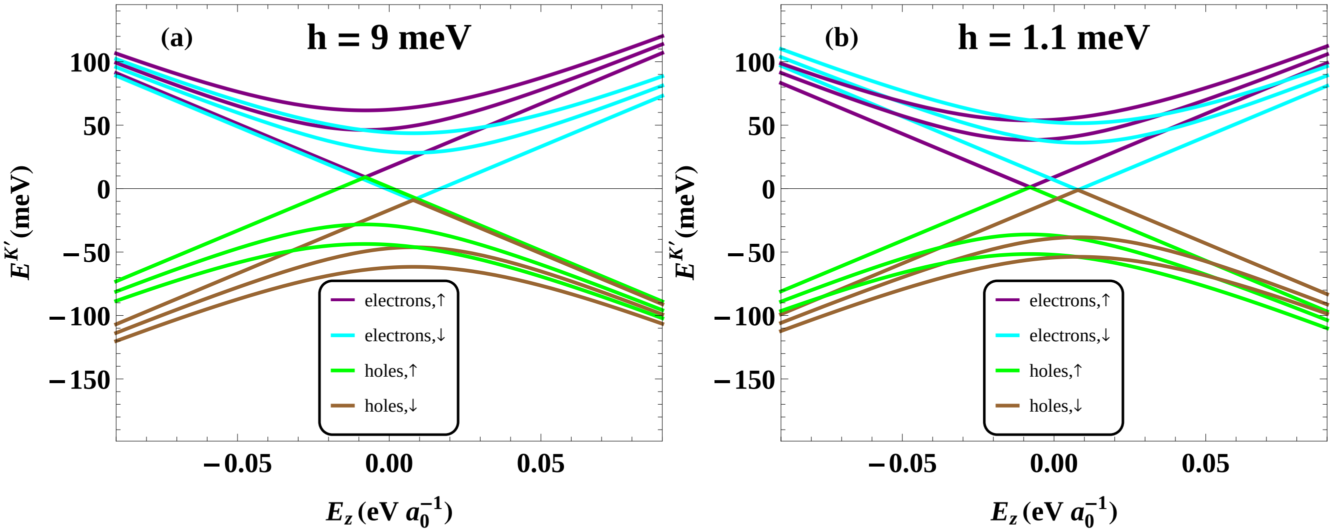

Figure 2.2: Energy dispersion for K' valley, varying with perpendicular electric field. $\Delta_{so} = 7.9meV$, $B = 4.1T$, $a_0 = 0.23A^0$.

2.3.1 Berry Curvature

Similar to gauge field tensor in electrodynamics, Berry curvature is a gauge-field tensor. It is gauge invariant and thus observable. In addition to electron dynamics, Berry curvature plays a major role in transport properties and thermodynamic behavior of materials.

Generally Berry curvature can be calculated from the Kubo formula of conductivity (based on the linear response theory)[70].

$$\Omega^n_{\mu_1\mu_2} = \frac{i\sum_{n\neq n'}\langle n|\frac{\partial H}{\partial R^{\mu_1}}|n'\rangle\langle n'|\frac{\partial H}{\partial R^{\mu_2}}|n\rangle - (\mu_2 \leftrightarrow \mu_1)}{(E_n - E_{n'})^2}. \tag{2.7}$$

Physically, Berry curvature is similar to magnetic field in momentum space. Therefore, even with no external magnetic field, the Berry curvature can induce transverse motion of the electrons. Hence the Hall response can appear for each single electron state.

For Landau levels greater than zero, the orthogonality of Hermite polynomials leads to:

$$\Omega^\alpha_{\sigma_z} = \frac{\alpha\hbar^2 v^2 \sin^2(\theta_n)}{2}\left(\frac{1}{\sqrt{n\Delta_B^2 + (\Delta_{so}\sigma_z - \Delta_z\alpha)^2} + \sqrt{(n+1)\Delta_B^2 + (\Delta_{so}\sigma_z - \Delta_z\alpha)^2}}\right)^2. \tag{2.8}$$

The appearance of α in the above expression is very important because it makes the Berry curvature strictly valley dependent. It is clear from Fig.(2.3) that

$$\Omega^K_\uparrow = -\Omega^{K'}_\downarrow, \Omega^K_\downarrow = -\Omega^{K'}_\uparrow. \tag{2.9}$$

As Berry curvature appears to be independent of exchange field, changing its value does not affect the magnitude and behavior of Berry curvature as shown in Figs. 2.3(a). Berry curvature can be tuned with externally applied electric field. Therefore, physical quantities related to Berry curvature are tunable. Valley Berry curvature can be calculated with the wave functions is calculated

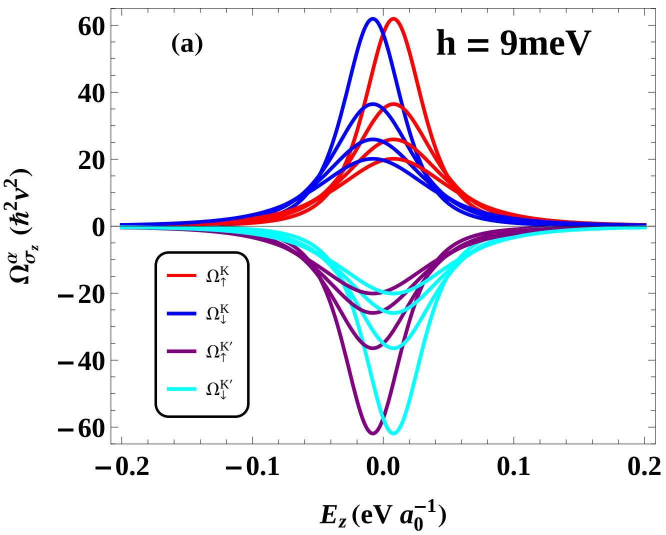

Figure 2.3: Berry curvature in the units of $\hbar^2 v^2$, with varying electric field. Taking $\Delta_{so} = 7.9meV$.

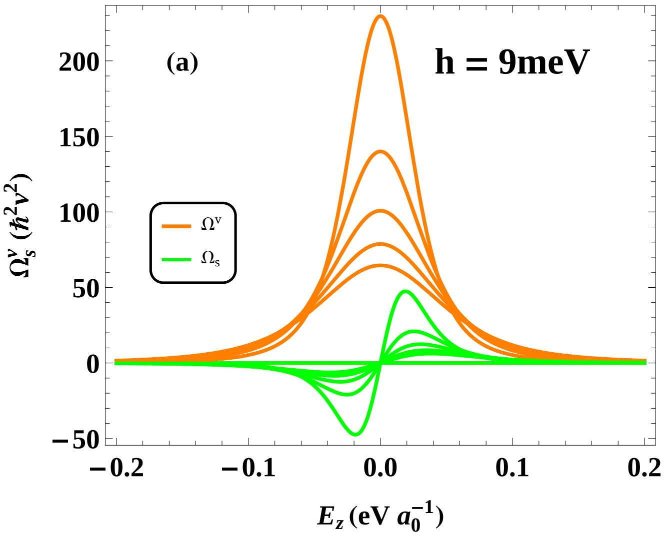

Figure 2.4: Valley Berry curvature (orange) and spin Berry curvature (green), in the units of $\hbar^2 v^2$, with varying electric field. Taking $\Delta_{so} = 7.9meV$.

by subtracting Berry curvatures of the two valleys as shown in Fig.(2.4) (orange). It is seen that the lower Landau levels contribute major part when electric field is varied, higher Landau levels have a constant background contribution and do not show sharp tuning with electric field. Both spin (green) and valley (orange) Berry curvatures can be controlled by an applied electric field. As shown, spin Berry curvature can be flipped by changing the direction of the applied electric field.

2.3.2 Magnetic Moment

Magnetic moments can be expressed in terms of Berry curvature as [70].

$$m^{\alpha}_{\sigma_z} = \frac{e}{\hbar}(E^{\alpha}_{\sigma_z}\Omega^{\alpha}_{\sigma_z}). \tag{2.10}$$

Using this relation we have calculated the magnetic moment to be:

$$m^{\alpha}_{\sigma_z} = \alpha \frac{e}{\hbar} \frac{\hbar^2 v^2 \sin^2\theta_n}{2} \left(\frac{\left(h\sigma_z + s\sqrt{n\Delta_B^2 + (\Delta_{so}\sigma_z - \Delta_z\alpha)^2}\right)}{\left(\sqrt{n\Delta_B^2 + (\Delta_{so}\sigma_z - \Delta_z\alpha)^2} + \sqrt{(n+1)\Delta_B^2 + (\Delta_{so}\sigma_z - \Delta_z\alpha)^2}\right)^2} \right) \tag{2.11}$$

As required by time-reversal symmetry orbital magnetic moments in both valleys have opposite signs. Non-zero magnetic moments show the magnetic behavior of silicene. The magnetic moment depends on SOC, electric field interaction, exchange field and valley degree of freedom. For a gapped system, there can be a magnetic moment that depend strictly on the valley degree of freedom, similar to a magnetic moment associated with real spin. This behaves similar to real spin and can give a Zeeman like contribution to energy. Hence, this magnetic moment contribution is related to valley orbit locking.

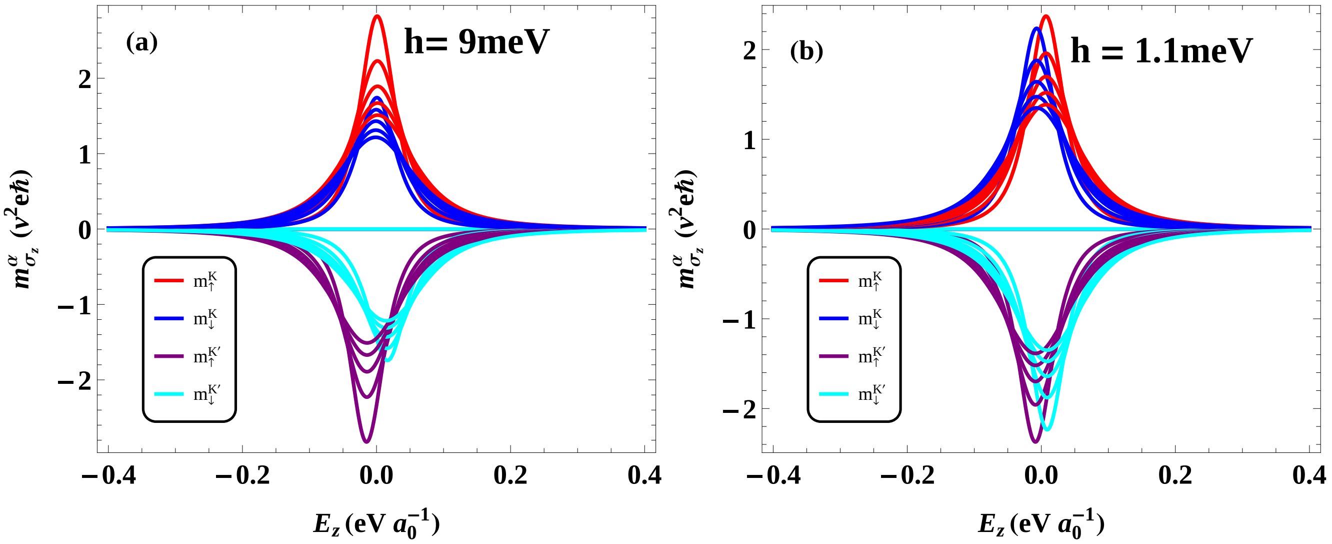

Figure 2.5: Magnetic moment as a multiple of $v^2 e/\hbar$ with varying E_z.

Magnetic moments for both valleys, keeping SOC constant can be seen in Fig. 2.5. Two important and interesting implications are there. Firstly, the magnetic moment associated with the orbital motion of Bloch bands can be adjusted externally. Here external electric field is the tuning parameter which can tune the magnetic moment from zero to a maximum value. These valley dependent magnetic moments are proposed to be used in valleytronics. Secondly, Fig. 2.5 shows that exchange field favors up spin for both valleys and shift the peak of K valley to zero electric field. Thus the exchange field of $9meV$ has influence not only on the spin, but on the valley too, leading to valley spin locking. Therefore, tuning the proximity exchange field and electric field gives control of both degrees of freedom.

Figs. 2.6 (a) and (b) show the dependence of net magnetic moment on exchange field. Net valley magnetic moment is obtained by subtracting the moments of both valleys. This effective valley magnetic moment is maximum with zero electric field, i.e. it is caused by SOC only. Net valley and spin magnetic moments both can be tuned with external electric field. The spin magnetic moment graph shows strong dependence on electric field. The amount by which up spin is favored

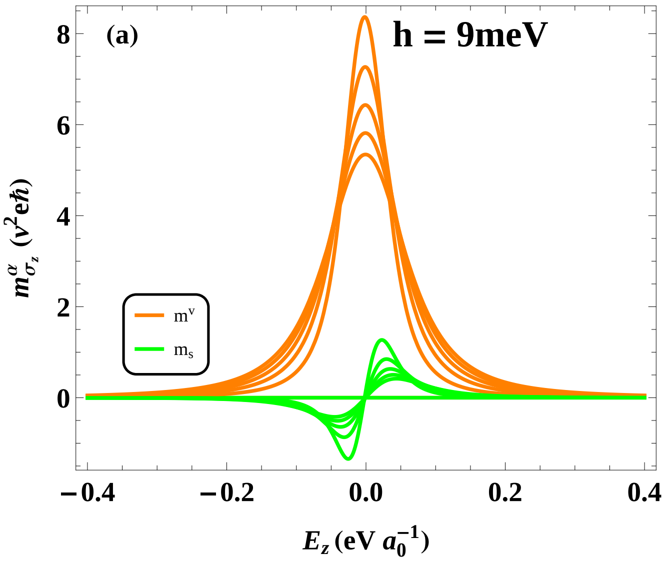

Figure 2.6: Valley magnetic moment (orange) and spin magnetic moment (green), in the units of $v^2 e/\hbar$, with varying E_z.

gets balanced by the amount, the down spin is suppressed. Interplay between SOC and electric field give rise to spin magnetic moment which can be used to reverse its direction. The magnetic moment can be experimentally observed if we apply time varying magnetic field B' to couple with magnetic moment. This will cause energy to shift by the amount $m.B'$, a Zeeman like term.

2.3.3 Valley polarization

In transition metals dichalcogenides valley polarization is proposed to be controlled due to valley contrasting orbital magnetic moment, which is generated using circularly polarized light in TMD[76] and through elliptical pumping[100]. Here strong SOC and electric field plays a vital role in tuning the valley polarization. Valley polarization is calculated in a similar way as spin polarization:

$$P_v = \frac{\rho_+ - \rho_-}{\rho} \tag{2.12}$$

ρ_+ is an electron density in the K valley and ρ_- in K' and ρ is the total carrier density of electrons.

The electron density is obtained by integrating the density of states modified by Berry curvature; as in semi classical theory[76, 101]

$$\rho(\zeta, \alpha, \sigma_z) = \int^{\zeta} \frac{d^2k}{(2\pi)^2} \left(1 + \frac{B.\Omega}{\hbar}\right) f(k, \alpha, \sigma_z). \tag{2.13}$$

Here $f(k, \alpha, \sigma_z)$ is the Fermi Dirac distribution function. ζ is the chemical potential. Valley polarization is non-zero due to orbital contribution of the magnetic moment and difference in the electron density of the two valleys. Fig. 2.7 demonstrates the non-zero valley polarization when chemical potential is below $0.1eV$. This shows that for higher chemical potential there was no net accumulation of electrons in one valley, but below $0.1eV$ there is a jump towards constant polarization of electrons. For energy greater than $0.1eV$ the drop of polarization in

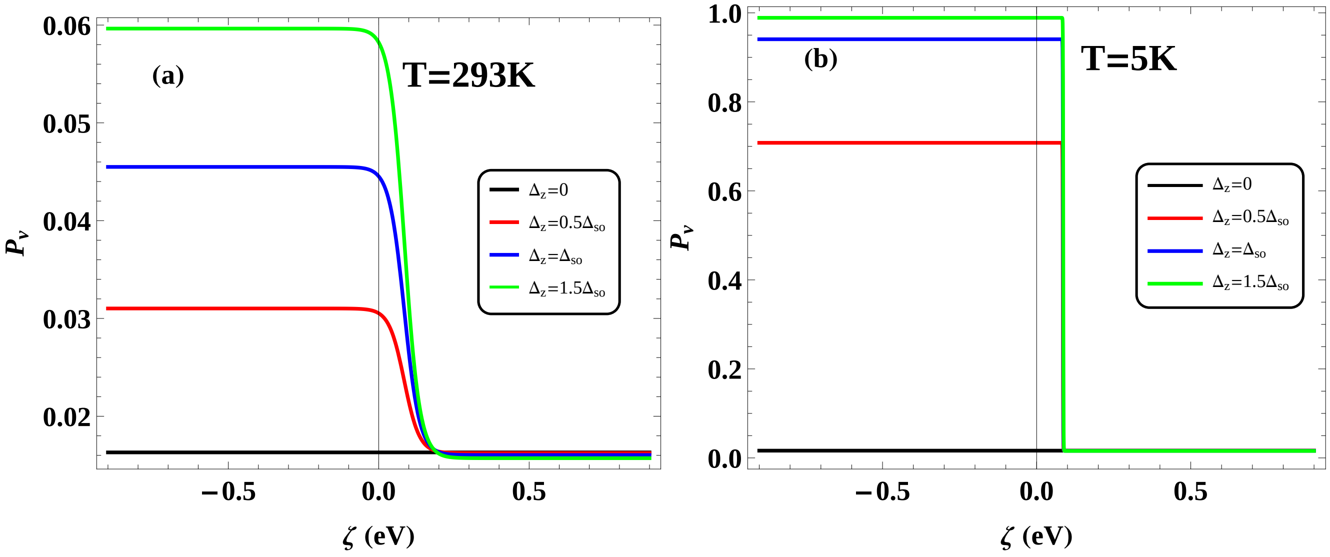

Figure 2.7: Variation of valley polarization as a function of chemical potential (eV). Taking $\Delta_{so} = 7.9meV$, $h = 1.1meV$ and $B = 1T$.

valleys is due to non availability of higher states as magnetic field is fixed at $1T$. It can be seen in Fig. 2.7 that application of electric field is important for non-zero valley polarization. An important feature is non dependence of valley polarization on proximity exchange field. This net polarization of electrons in one valley relative to the other is the cause of appearance of valley Hall conductivity. This contribution is proposed to be detected experimentally in valley half metals[82], thus validating the contribution and role of valley degree of freedom for possible use in valleytronics.

2.3.4 Valley and spin Hall conductivities

Another possible way to observe the phase transitions and valley dependent behavior of silicene is to measure the Hall conductivity. Using Kubo formalism, Hall Conductivity is

$$\sigma_{xy} = \frac{i\hbar e^2}{L_x L_y}\sum_{n\neq n'}[f(E_n)(1-f(E_{n'}))]^*\left\langle n\middle|v_x\middle|n'\right\rangle\left\langle n'\middle|v_y\middle|n\right\rangle\frac{1-exp\left(\frac{E_n-E_{n'}}{k_BT}\right)}{(E_n-E_{n'})^2} \tag{2.14}$$

which can be simplified as

$$\begin{aligned}\sigma_{xy} &= A_2\Bigg[\frac{1}{1+exp(\frac{b+\sqrt{n\Delta_B^2+(\Delta_{so}\sigma_z-\Delta_z\alpha)^2}-\zeta}{k_BT})}-\frac{1}{1+exp(\frac{b+\sqrt{(n+1)\Delta_B^2+(\Delta_{so}\sigma_z-\Delta_z\alpha)^2}-\zeta}{k_BT})}\\ &+ \frac{1}{1+exp(\frac{b-\sqrt{n\Delta_B^2+(\Delta_{so}\sigma_z-\Delta_z\alpha)^2}-\zeta}{k_BT})}-\frac{1}{1+exp(\frac{b-\sqrt{(n+1)\Delta_B^2+(\Delta_{so}\sigma_z-\Delta_z\alpha)^2}-\zeta}{k_BT})}\Bigg]\end{aligned} \tag{2.15}$$

where $A_2 = \frac{\alpha e^2\sin^2\theta_n}{\hbar}\left[n+\frac{1}{2}+\left(\frac{\Delta_{so}\sigma_z-\Delta_z\alpha}{\Delta_B}\right)^2\right]$.

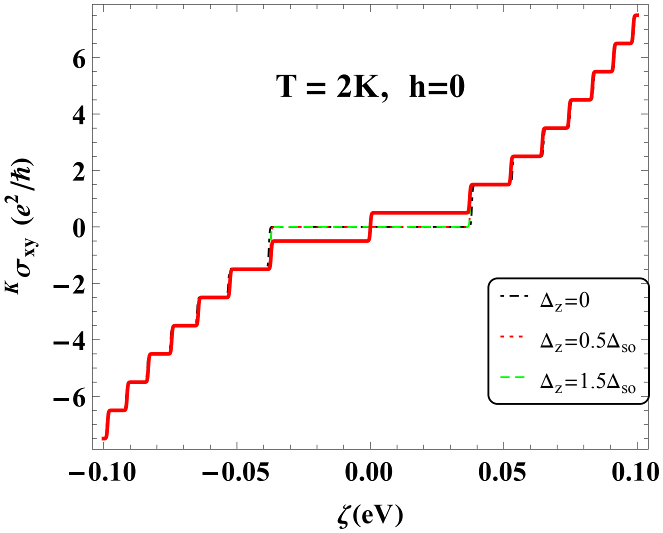

Figure 2.8: Hall conductivity in K valley (for spin up) as a multiple of $e^2/\hbar$. Taking $h = 0meV$ and $\Delta_{so} = 7.9meV$. Red plot is for $\Delta_z = \Delta_{so} = 0$ (semimetallic state)

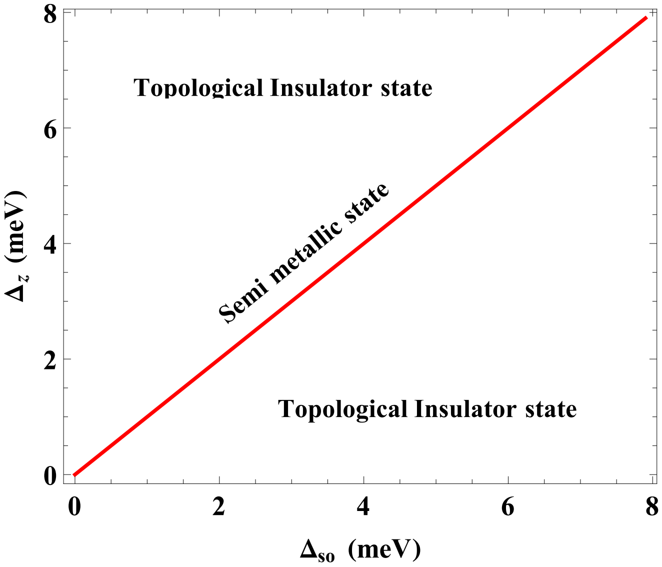

Figure 2.9: Phase diagram of silicene showing semi metallic state for $\Delta_z = \Delta_{so}$, topological insulator state for$\Delta_z < \Delta_{so}$ and $\Delta_z > \Delta_{so}$.

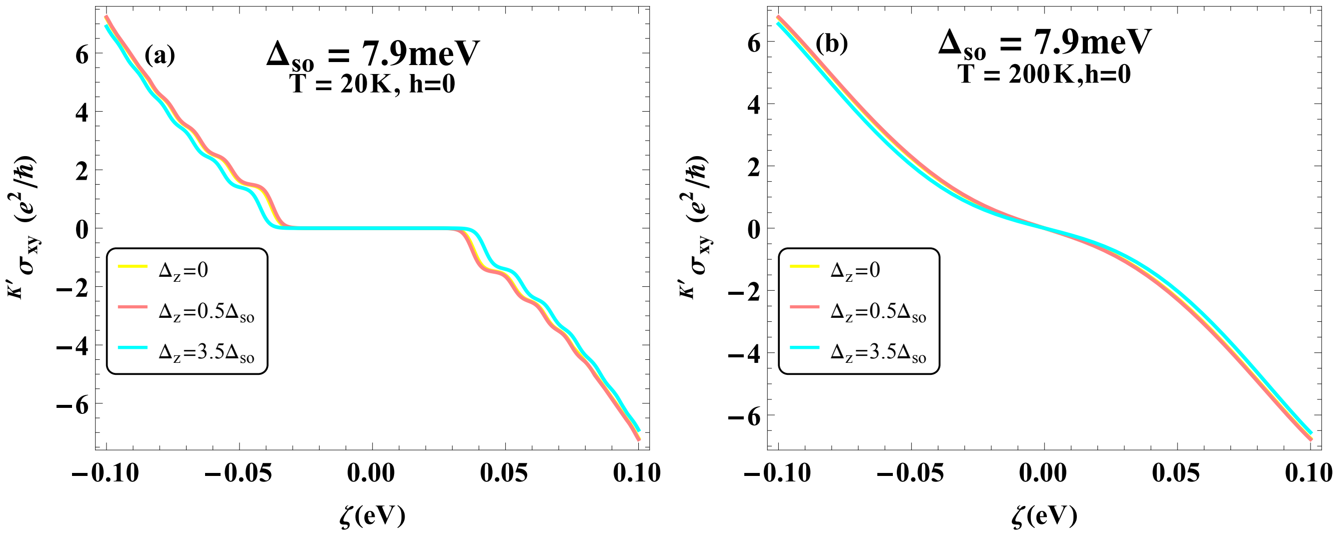

Figure 2.10: Hall conductivity in K' valley (for spin down) as a multiple of $e^2/\hbar$.

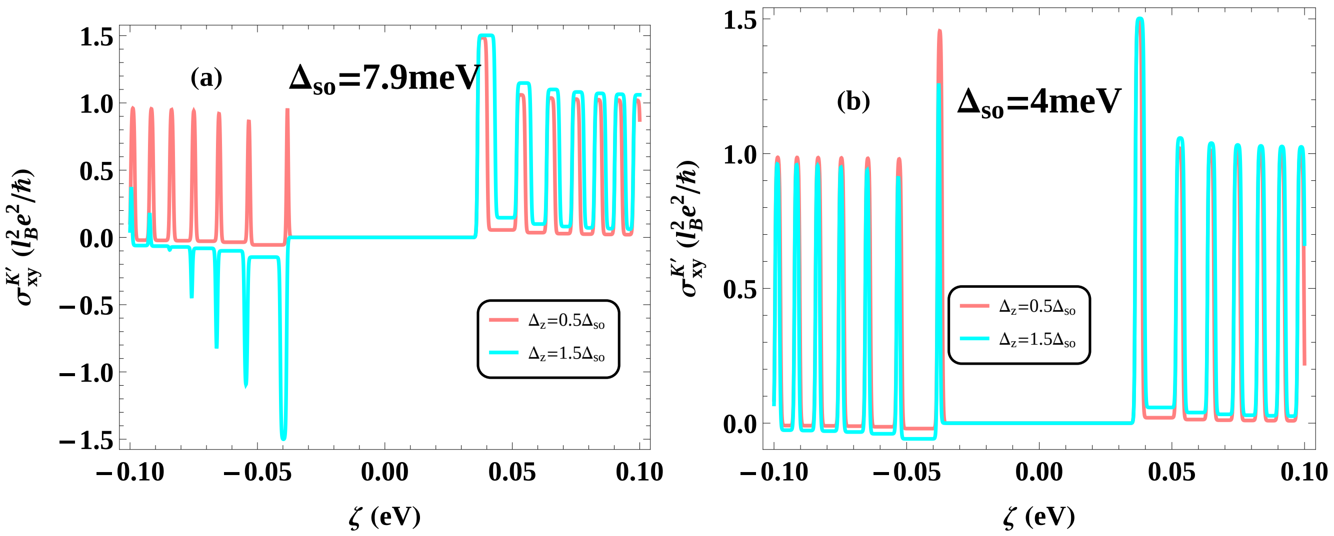

Figure 2.11: Spin Hall conductivity for K' valley as a multiple of $l_B e^2/\hbar$ with $B = 4.1T$, $h = 1.1meV$ and $T = 2K$.

Hall conductivity for K valley (spin up) is equal to negative of the Hall conductivity for K' valley (spin down) and vice versa. Hall conductivity at charge neutrality point is zero for topological insulator and has a finite value (red) for the semimetallic phase, due to band inversion, as shown in Fig. 2.8. The transition is mainly due to the contribution and vital role of zeroth Landau level.

When silicene is not in proximity with a magnetic material, changing the electric field causes the appearance of phase transition for $\Delta_z = \Delta_{so}$. Experimentally Hall conductivity is measured as a function of the gate voltage and it tunes the chemical potential. For silicene net Hall conductivity appears to be zero showing exactly opposite behavior of electrons for both valleys. At high temperature the phase transition disappears as shown in Fig. 2.10(b). An additional feature of higher

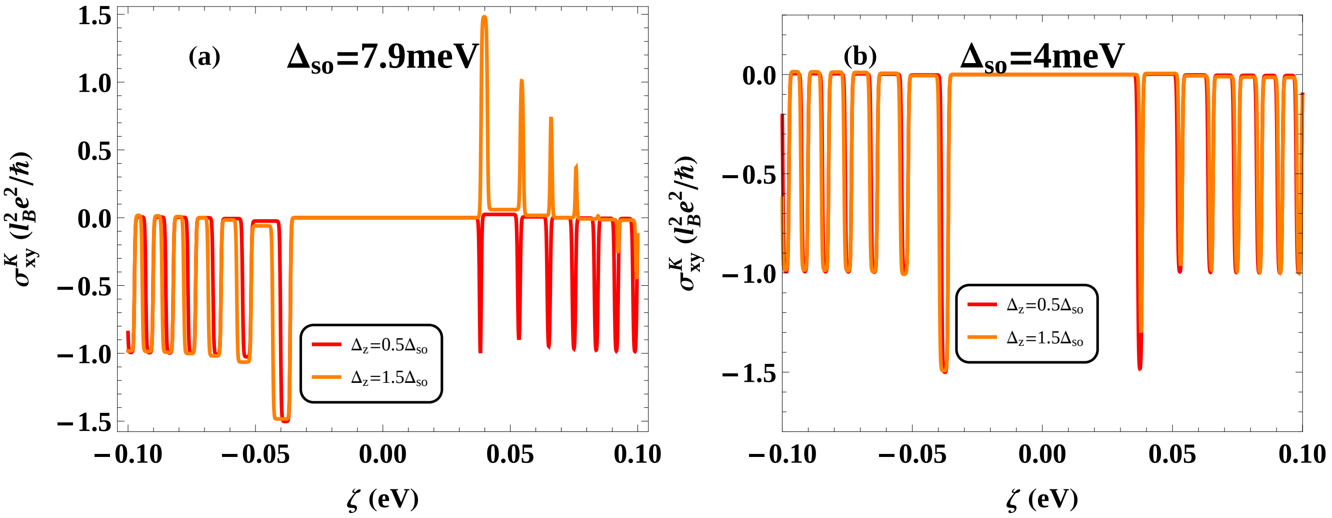

Figure 2.12: Spin Hall conductivity for Kvalley as a multiple of $l_B e^2/\hbar$ with $B = 4.1T$, $h = 1.1meV$ and $T = 2K$.

temperature is that Hall conductivity does not remain quantized as shown in Fig. 2.10(b). So to observe the quantization in Hall conductivity and the phase transition, low temperature is required.

Spin Hall conductivity is calculated by subtracting Hall conductivity due to one spin from the Hall conductivity due to opposite spin, keeping track of valley contributions. As chemical potential goes beyond $0.03eV$ non-zero spin Hall conductivity appears with sharp peaks for each Landau level. When $\Delta_{so} = 7.9meV$, spin Hall conductivity for $K(K')$ shows opposite behavior for $\Delta_z < \Delta_{so}$ and $\Delta_z > \Delta_{so}$ for positive (negative) chemical potential, showing the contribution from conduction (valence) electrons as shown in Fig.2.11(a) and Fig. 2.12(a). By decreasing the SOC to $\Delta_{so} = 4meV$ Fig. 2.11and Fig. 2.12(b) show opposite behavior for K and K' valley and the corresponding phase transition.

Spin Hall conductivity is non zero even with net zero Hall conductivity. Spin Hall conductivity shows oscillatory behavior but close examination shows that for particular values of Landau levels there are peaks. The overall change in spin conductivity caused by exchange field of one valley cancels the change in spin conductivity of other valley, thus making total spin conductivity independent of exchange field. Valley Hall conductivity is calculated by subtracting Hall conductivity due to one valley from the Hall conductivity due to the other valley, keeping track of both spin contributions. The non-zero valley Hall conductivity appear as steps, which is an indication of Landau levels or quantization of valley Hall Conductivity. It is a trivial insulating phase. So it can be concluded that net valley Hall conductivity appeasr to be non-zero in silicene. Non-zero valley and spin Hall conductivities show the accumulation of charges not only at the edges of opposite valleys but of opposite spins too.

2.4 Results

Magnetic and transport properties of silicene in the presence of perpendicular electric and magnetic fields as well as proximity to ferromagnetic material are studied. It is shown that for small exchange field, the magnetic moment associated with each valley is opposite and it gives a shift in band energy, by a Zeeman-like coupling term. Thus opening a new horizon for valley-orbit coupling. Magnetic proximity effect is shown to influence the spin state of each valley. Valley polarization can be modified and measured. Its contribution in Hall conductivity is illustrated. Quantum phase transitions are observed in silicene, providing a tool to control the topological state experimentally. The strong dependence of the physical properties on valley degree of freedom is an important step towards valleytronics.

Chapter 3

Response of Weyl semimetals to Broken Time Reversal Symmetry

3.1 Introduction

The study of topological properties of materials has gained momentum after the discovery of topological insulators due to their non trivial band structure. They have gapless edge states with gapped bulk and their response can be expressed in terms of topological invariants[9]. Topological insulators have been studied extensively but a new class of materials which are of great interest are topological semimetals; whose response is also characterized by topological invariants. They have gapless bulk and non degenerate valence and conduction bands touching at certain points or on a line in the Brillouin zone. They include materials with four energy bands having single point degeneracy in momentum space known as Dirac semimetals[20, 21, 22]. Dirac semimetals are time reversal and spatial inversion symmetric. When either symmetry is broken four fold degeneracy shifts to double degenerate points known as Weyl nodes and such point nodal materials are called Weyl semimetals. They are realized in pyrochlore iridates and were predicted based on calculations involving electron correlations and spin orbit coupling effects. $TaAs$ was the first Weyl semimetal discovered [56] and the predicted Fermi arcs were detected using photoemission spectrosopy and confirmed by first principles calculations[102]. Weyl semimetals and are classified into two types on the basis of respecting Lorentz symmtery (type I) [9, 52, 56] and not respecting Lorentz symmtery (typeII)[19]. $TaAs$[102, 103], $MoTe_2$[19], transition-metal monophosphides[52] are examples of topological semimetals.

Weyl semimetals have been proposed to appear in a multilayer model with alternating layers of ordinary insulator and TI. Normal insulator acts as a spacer between TI layers [51, 18]. Finite tunneling is allowed between top and bottom layers of TI layer and between two adjacent TI layers as shown in Fig. 3.1. As Dirac nodes must occur in pairs, this system has minimum number of two Dirac nodes. If the TI layers doped with magnetic atoms it give rises to semimetallic phase. This phase can have nodal or along the line degeneracy depending on the direction of the spin of dopant. In addition to Weyl semimetals these types of semimetals in which degeneracy occurs along a line are called line node semimetals. This multilayer model is employed in this chapter to discuss the magnetic response of Weyl semimetals.

Interesting effects are observed when topological semimetals are placed in an external magnetic field. One must keep in mind that magnetic field couples with both orbital (through minimal coupling) and spin degree of freedom (Zeeman coupling) of electrons. In the case of out of plane magnetic field, Landau levels appear whereas for in-plane magnetic field Dirac cones of the two surfaces shift in momentum space. Pyrochlore iridates are used as a reference Weyl semimetals to study the properties like anisotropy in longitudinal conductivity and dependence of velocity on the direction of applied magnetic field[104]. Many other anisotropic properties depending on magnetic field and chiral anomaly related phenomenon have been investigated[105, 106, **?**, 107, 108, 109]. Recently superconducting behavior of Weyl semimetals have been discussed with reference to the tilt angle[110, 111].

In this chapter we present magnetic response of topological semimetals in a tilted magnetic field, Zeeman coupling and orbital contribution taken into account. Our focus will be the study of magnetic susceptibility for different orientations of external magnetic field, with the focus on anisotropic magnetic response of Weyl semimetals. The magnetic susceptibility has three contributions arising from spin, spin-orbital and orbital motion. We show that (i) spin susceptibility scales linearly with the Fermi energy and can vanish for large deviation of the magnetic field from the perpendicular, (ii) spin-orbit susceptibility is an even function of Fermi energy and deviation angle of magnetic field. It strongly depends on the position of Fermi energy and can be paramagnetic or diamagnetic depending on it, (iii) orbital susceptibility is strongly diamagnetic and diverges if the Fermi level is at the charge neutrality point. This behavior has some similarity with that observed in nodal semimetals[112] and graphene[113]. We show that magnetic response can be distinguished by varying the magnetic field orientation. The study is divided into two parts with reference to the magnetic field orientation. One is the case of Landau Levels (LLs) formation (out of plane magnetic field), presented in sec.(3.2) and the second when energy spectrum is momentum dependent (in-plane magnetic field), presented in sec.(3.4).

3.2 Model for Weyl semimetals in a tilted magnetic field

We consider a heterostructure of alternating thin films of topological insulators (TI) and normal insulators (NI) lying in the xy-plane, in a magnetic field which is tilted at an angle θ with respect to the perpendicular axis which we take to be the z-axis, as shown in Fig. 3.1. Magnetic field has both inplane and out of plane components and is taken to be $\boldsymbol{B} = (\frac{Bsin\theta}{\sqrt{2}}, \frac{Bsin\theta}{\sqrt{2}}, Bcos\theta)$. As mentioned in the introduction that breaking TRS leads to appearance of Weyl semimetal phase and application of magnetic field fulfills the requirement. The effective low energy Hamiltonian[51] for our system is

$$H = v\tau_z\left(\hat{z}\times\sigma\right)\cdot\left(-i\hbar\overrightarrow{\nabla} + e\overrightarrow{A}\right) + \frac{g\mu_B B\cdot\sigma}{2} + \hat{\Delta}_D(k_z) \tag{3.1}$$

where $\overrightarrow{A} = (\frac{-yBcos\theta}{2} + \frac{zBsin\theta}{\sqrt{2}}, \frac{xBcos\theta}{2} - \frac{zBsin\theta}{\sqrt{2}}, 0)$ is the vector potential for the tilted magnetic field[114]. σ and τ are Pauli matrices for spin and surface pseudospin, v is Fermi velocity of electrons, g is the gyromagnetic ratio, μ_B is the Bohr magneton, $\hat{\Delta}_D(k_z) = \Delta_t\tau_x + \frac{1}{2}\Delta_N(\tau_+ \exp^{ik_z d} + \tau_- \exp^{-ik_z d})$, where $\tau_\pm = \tau_x \pm i\tau_y$. The first term in Eq.3.1 is the kinetic energy contribution, second is the Zeeman term and the last term arises due to tunneling of electrons between the different layers. Δ_t is the tunneling amplitude between the top and bottom of TI film and Δ_N is the tunneling amplitude arising due to tunneling across the NI layer.

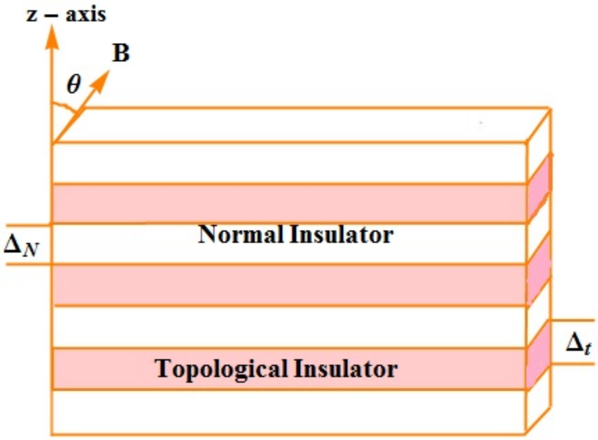

Figure 3.1: Schematic diagram of the system showing alternate monolayers of topological insulator and normal insulator in magnetic field B tilted at angle θ.

The inplane magnetic field acts to shift Dirac cones of the two surfaces of topological insulator along the y-axis[115, 116]. To incorporate this effect and to determine the energy spectrum we define creation and annihilation operators for the two surfaces:
$\pi_{y_i} - i\pi_{x_i} = -\frac{i\sqrt{2}\hbar}{l_B}a_i^\dagger$ and $\pi_{y_i} + i\pi_{x_i} = \frac{i\sqrt{2}\hbar}{l_B}a_i$, where

$\pi_{x_1} = v(p_x + e(zb_1 - yb_2) + \frac{cb_1}{v})$,
$\pi_{y_1} = v(p_y + e(-zb_1 + xb_2) + \frac{cb_1}{v})$,
$\pi_{x_2} = v(p_x + e(zb_1 - yb_2) - \frac{cb_1}{v})$,
$\pi_{y_1} = v(p_y + e(-zb_1 + xb_2) - \frac{cb_1}{v})$,
$c = \frac{g\mu_B}{2}$, $b = cB$, $b_1 = \frac{Bsin\theta}{\sqrt{2}}$, $b_2 = \frac{Bcos\theta}{2}$.

The Hamiltonian in Eq. 3.1 can be conveniently re-expressed as

$$H = \begin{pmatrix} bcos\theta & -i\Delta_B a_1 & \Delta & 0 \\ i\Delta_B a_1^\dagger & -bcos\theta & 0 & \Delta \\ \Delta^* & 0 & bcos\theta & i\Delta_B a_2 \\ 0 & \Delta^* & -i\Delta_B a_2^\dagger & -bcos\theta \end{pmatrix} \tag{3.2}$$

where $\Delta = \Delta_t + \Delta_N exp^{ik_z d}$, $\Delta^* = \Delta_t + \Delta_N exp^{-ik_z d}$, $\Delta_B = \frac{\sqrt{2}\hbar}{l_B}$ and $l_B = \sqrt{\frac{\hbar}{eBcos\theta}}$ is the magnetic length. For $n \geq 1$, the eigenfunctions can be written as

$C_1\Phi_n|T\uparrow\rangle + C_2\Phi_{n-1}|T\downarrow\rangle + C_3\Phi_n|B\uparrow\rangle + C_4\Phi_{n-1}|B\downarrow\rangle$. The corresponding energy spectrum is then given by

$$E_{s,\mu}(n) = s\sqrt{\Delta_B^2 n + (b\cos\theta + \mu\Delta_D)^2}, \tag{3.3}$$

where $\Delta_D(k_z) = \sqrt{\Delta_N^2 + \Delta_t^2 + 2\Delta_t\Delta_N\cos(k_z d)}$. $s = +1$ for conduction and -1 for valence band, n is the Landau level index and $\mu = \pm$ determining the sub-splitting of LLs.

It is evident from Eq. 3.3 that crossing points of $n = 0$ Landau level appear due to interplay of Δ_D, b and tilt angle θ. The $n = 0$ LL does not split into four sublevels like $n \neq 0$ levels due to "zero-mode anomaly"[117]. Thus out of four two energy levels exist and two do not exist. Former are called existing LLs and later are called non existing LLs. When $b\cos\theta < \Delta_D$ the two corresponding energy levels are particle-hole symmetric

$$E_{+1,-1} = |b\cos\theta - \Delta_D|, E_{-1,+1} = -|b\cos\theta + \Delta_D| \tag{3.4}$$

whereas for $b\cos\theta > \Delta_D$, the energy levels are both hole-like

$$E_{-1,-1} = -|b\cos\theta - \Delta_D|, E_{-1,+1} = -|b\cos\theta + \Delta_D| \tag{3.5}$$

which means that $n = 0$ and $\mu = -1$ energy level shifts from electron like to hole like energy level resulting in an extra filled LL and nonzero Hall conductance. It can be seen from Fig. 3.2 that the results for $\theta = 0$ matches with the results obtained previously[18]. Fig. 3.2 shows the energy spectrum as a function of applied magnetic field for different tilt angles. In Fig. 3.3, we show the evolution of $n = 0$ LLs as a function of the strength (magnitude) and orientation of the applied magnetic field. By tuning the magnetic field and its orientation, the $n = 0$ LLs shift from electron-like to hole-like. It can be seen in Fig. 3.4 that for different magnetic field strength appearance of nodes depend on the condition $\mid \Delta_t - \Delta_N \mid < b\cos\theta < \Delta_t + \Delta_N$. By keeping in mind the appearance of existing and nonexisting energy levels for $n = 0$, we can write Eq.(3.6) for the case when $b\cos\theta > \Delta_D$ as

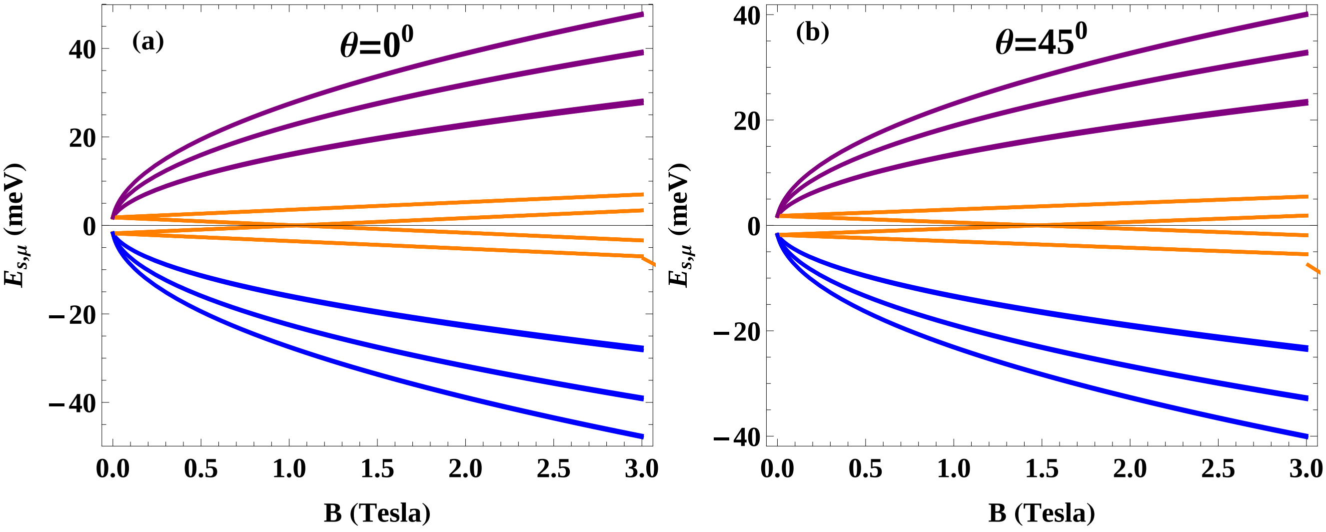

Figure 3.2: Energy spectrum with magnetic field at (a) $\theta = 0^0$ and (b) $\theta = 45^0$. Here $b = 1.73BmeV$, $\Delta_D = 1.8meV$ for$k_z = 0$, $\Delta_t = 1meV$ and $\Delta_N = 0.8meV$.

$$E_{s,\mu}(0) = \lambda_{s,\mu} E_\mu \tag{3.6}$$

where $E_\mu = -(b\cos\theta - \mu\Delta_D)$ $\lambda_{s,\mu} = +1$ for existing energy levels and $\lambda_{s,\mu} = -1$ for nonexisting energy levels whereas for $b\cos\theta < \Delta_D$ Eq.(3.4) can be written as

$$E_{s,\mu}(0) = \lambda_{s,\mu} E_s \tag{3.7}$$

where$E_s = sb\cos\theta - \Delta_D$.

In the next section magnetic susceptibility for our system is calculated.

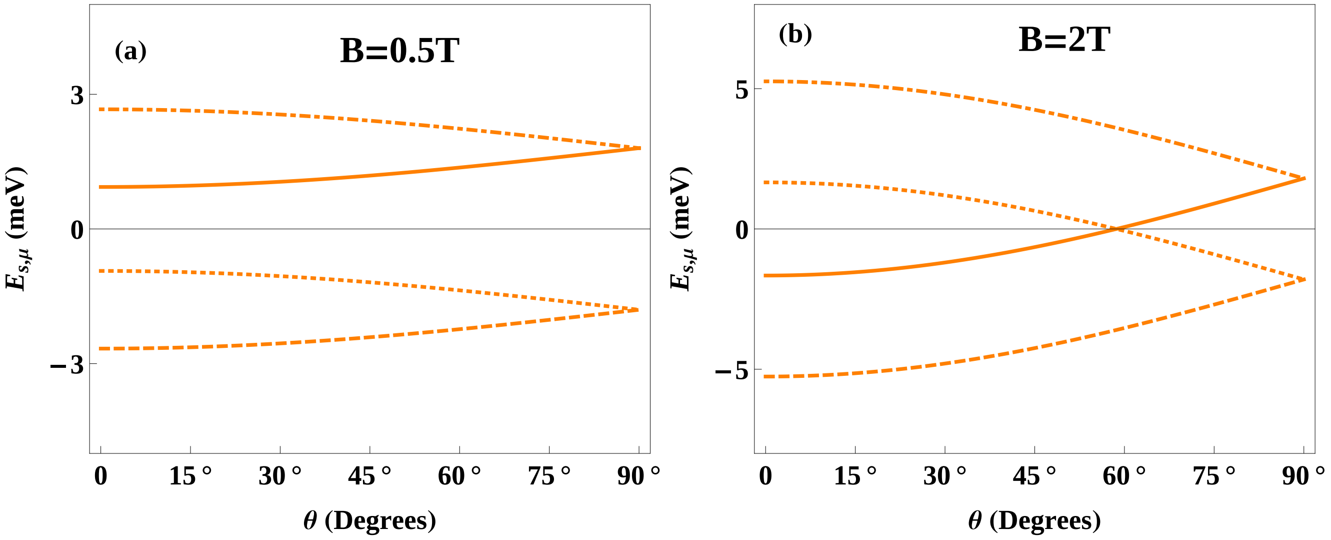

Figure 3.3: Variation of energy for $n = 0$ LL with the tilt angle θ of the applied magnetic field (a) $B = 0.5T$ and (b) $B = 2T$. Here $b = 1.73BmeV$, $\Delta_D = 1.8meV$ for $k_z = 0$, $\Delta_t = 1meV$ and $\Delta_N = 0.8meV$. Dotted curve represents $E_{+,-}$, thick curve represents $E_{-,-}$, dot-dashed curve represents $E_{+,+}$ and dashed curve represents $E_{-,+}$.

3.3 Magnetic susceptibility for tilted magnetic field

Magnetic susceptibility is a fundamental quantity that is needed to determine the magnetic response of a material. An applied Magnetic field couples with both orbital and spin motion and we treat both of them separately as B_o and B_s respectively. Mathematically magnetic susceptibility is obtained by differentiating the thermodynamical potential twice with respect to magnetic field. To keep things generic we have taken magnetic field to be oriented at some angle θ with respect to z-axis.

We have three susceptibility contributions: spin susceptibility (χ_s), spin-orbit susceptibility (χ_{so}) and orbital susceptibility (χ_o)[114]. They are obtained from the thermodynamical potential F defined as terms of partition function Z as,

$$F = -k_B T \ln Z$$
$$Z = \sum_i [1 + e^{-\beta(E_i - \zeta)}]$$

where $\beta = \frac{1}{k_B T}$, T is the temperature, k_B is the Boltzmann constant, E_i is the energy eigenvalue of the i^{th} state and ζ is the chemical potential. Magnetization M, can be written as a derivative of F, for $B_s = B_o = B$ as

$$M = -(\frac{\partial F}{\partial B_s} + \frac{\partial F}{\partial B_o}).$$

As χ is defined as the derivative of magnetization, we can write the above equation as

$$\begin{aligned} \chi &= -(\frac{\partial^2 F}{\partial B_s^2} + 2\frac{\partial^2 F}{\partial B_s \partial B_0} + \frac{\partial^2 F}{\partial B_0^2}) \\ &\equiv \chi_s + \chi_{so} + \chi_o. \end{aligned}$$

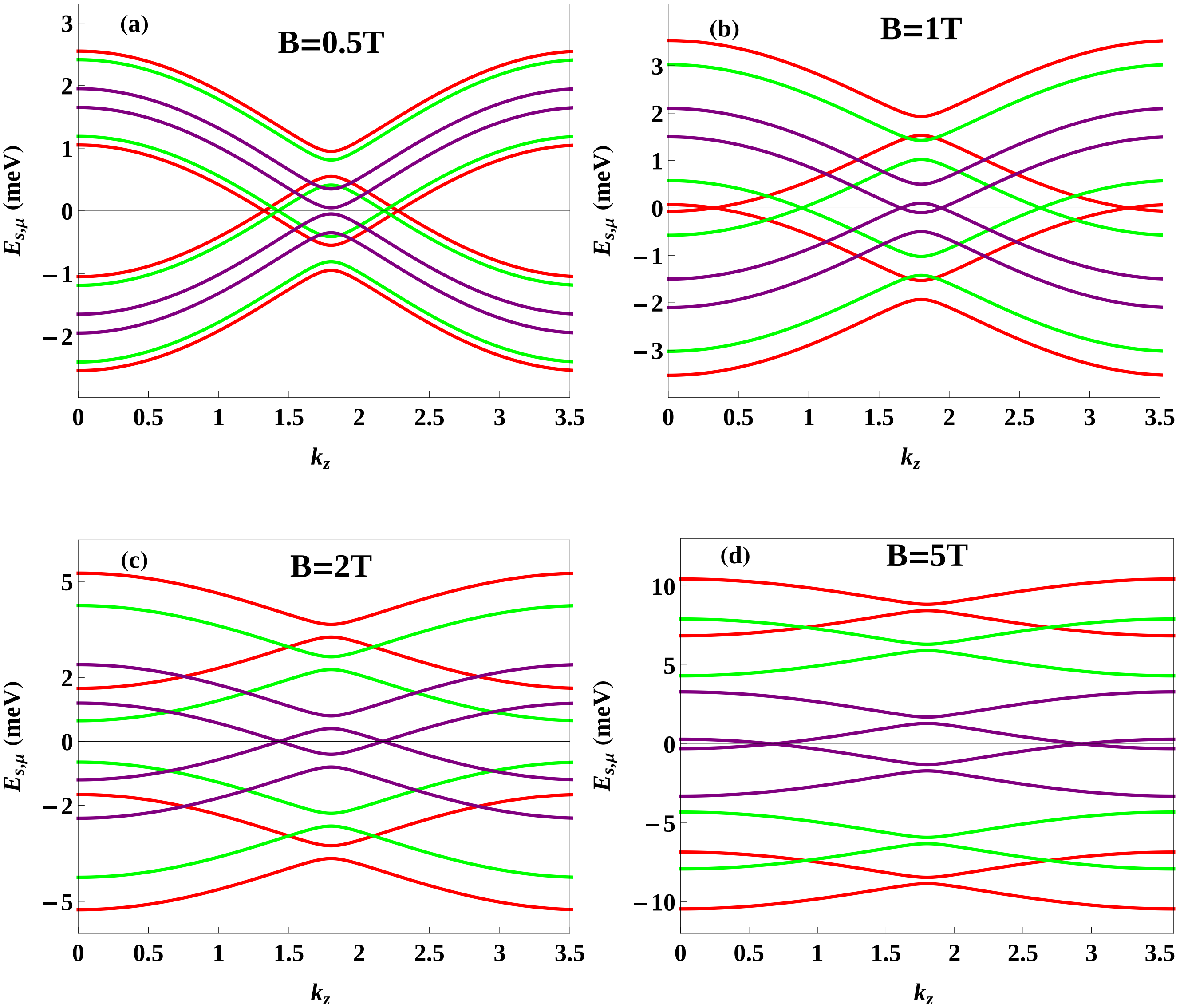

Figure 3.4: Variation of energy for $n = 0$ Landau level with k_z for different magnetic fields. Here $b = 1.73B meV$, $\Delta_t = 1meV$ and $\Delta_N = 0.8meV$. Colors used are red for $\theta = 0^0$, green for $\theta = 45^0$ and purple for $\theta = 80^0$.

For Landau level energy spectrum given in Eq.(3.3) thermodynamical potential is written as

$$F = -\frac{1}{\beta}\frac{1}{2\pi l_B^2}\sum_i \sum_{n=n'}^{\infty} \ln[1 + e^{-\beta[E_i(x_n)-\zeta]}] \tag{3.8}$$

where $n' = 0$ for existing and $n' = 1$ for nonexisting energy levels, n is the Landau level index, $x_n = n\Delta x$, $\Delta x = \frac{2(\hbar v)^2}{l_B^2}$ and l_B is the magnetic length.

The summation over n in Eq. 3.8 can be executed by employing the Euler-Maclaurin formula for the function defined above. It must be noted here that existing and nonexisting branches lead to sign reversal of second term, determined by λ :

$$\begin{aligned}\sum_{n=n'}^{\infty} y(x_n) &= \frac{1}{\Delta x}[\int_0^{\infty} y(x)dx + \lambda y(0)\frac{\Delta x}{2} \\ &- y'(0)\frac{\Delta x^2}{12} + O(\Delta x^3)]. \end{aligned} \tag{3.9}$$

Eq. 3.8 together with Eq. 3.9 yields

$$\begin{aligned} F &= -\sum_i \frac{1}{4\pi\hbar^2 v^2 \beta}\int_0^{\infty} \phi[E_i(x)]\,dx \\ &+ \lambda_i \phi[E_i(0)]\frac{e}{4\pi\hbar\beta}B_o \\ &- \phi'[E_i(0)]\frac{e^2v^2}{12\pi\beta}B_o^2 + O(\Delta x^2) \end{aligned} \tag{3.10}$$

where $\phi[E_i(x)] = \ln[1+e^{-\beta[E_i(x_n)-\zeta]}]$. From the above equation we can define the following parameters that will be needed in the calculation of susceptibility that follows:

$$\begin{aligned} \nu_0 &= -\frac{1}{\beta}\sum_i \frac{1}{4\pi\hbar^2 v^2}\int_0^{\infty} \phi[E_i(x)]\,dx, \\ \nu_1 &= -\frac{1}{\beta}\sum_i \lambda_i \phi[E_i(0)]\frac{e}{4\pi\hbar}, \\ \nu_2 &= \frac{1}{\beta}\sum_i \phi'[E_i(0)]\frac{e^2v^2}{12\pi}. \end{aligned}$$

It is evident that thermodynamic potential can be expanded in terms of orbital magnetic field component B_o

$$F = \nu_0 + \nu_1 B_o + \nu_2 B_o^2 + O(B_o^3) \tag{3.11}$$

Using Eq. 3.11 we can calculate susceptibility by differentiating F

$$\chi_s = -(\frac{g\mu_B}{2})^2\frac{\partial^2 \nu_0}{\partial b^2}, \tag{3.12}$$

$$\chi_{so} = -2\frac{g\mu_B}{2}\frac{\partial \nu_1}{\partial b}, \tag{3.13}$$

$$\chi_o = -2\nu_2. \tag{3.14}$$

where $\frac{\partial}{\partial B_s} = (\frac{g\mu_B}{2})\frac{\partial}{\partial b}$.
The different contributions to susceptibility are discussed in the following sections.

3.3.1 Spin susceptibility

Spin susceptibility is non-zero because of contribution from both Fermi surface states and occupied states. Thus we have Pauli and Van-vleck paramagnetic contributions in our expression from Eq. 3.12, written as

$$\begin{aligned} \chi_s &= -A_1 \sum_{s,\mu,k_z}\int_0^{\infty} \frac{(b\cos\theta + \mu\Delta_D)^2}{E^2_{s,\mu(x)}} f'[E_{s,\mu}(x)]\,dx \\ &+ \int_0^{\infty} (\frac{1}{E_{s,\mu}(x)} - \frac{(b\cos\theta+\mu\Delta_D)^2}{E^3_{s,\mu}(x)}) f[E_{s,\mu}(x)]\,dx \end{aligned} \tag{3.15}$$

where $A_1 = \frac{1}{4\pi\hbar^2 v^2}(\frac{g\mu_B}{2})^2$, $f[E_{s,\mu}(x)] = \frac{1}{[1+\exp^{\beta(E_{s,\mu}(x)-\zeta)}]}$ is the Fermi-Dirac distribution function. For $T \rightarrow 0$ Fermi function becomes a step function and its derivative a Dirac delta function:

$$f[E_{s,\mu}(x)] \rightarrow \Theta(E_f - E_{s,\mu}(x))$$

$$\sum_s \frac{f[E_{s,\mu}(0)]}{[E_{s,\mu}(0)} = \frac{\Theta(E_f - E_\mu(0))}{E_\mu(0)}$$

$$\frac{\partial f[E_{s,\mu}(x)]}{\partial E_{s,\mu}(x)} \rightarrow -\delta(E_f - E_{s,\mu}(x)).$$

Thus for $T \rightarrow 0$ the expression for χ_s from Eq. 3.15 after integration and using the above expressions become

$$\chi_s = -\sum_{k_z} \frac{E_f}{2\pi}\left(\frac{g\mu_B\cos\theta}{2\hbar v}\right)^2.$$

Using

$$\sum_{k_z} = \frac{1}{2\pi}\int_{-\infty}^{\infty} dk_z,$$

Carrying out the summation on k_z around the nodes yields

$$\chi_s = -\frac{E_f}{2\pi^2}(\frac{g\mu_B\cos\theta}{2\hbar v})^2 k_0, \tag{3.16}$$

where $k_0 = \frac{1}{d}\cos^{-1}[1 - \frac{(b\cos\theta)^2-(\Delta_t-\Delta_N)^2}{2\Delta_t\Delta_N}]$. It is clear that the expression for spin susceptibility depends linearly on Fermi energy E_f, on the orientation of magnetic field and on the condition that $\mid \Delta_t - \Delta_N \mid < b\cos\theta < \Delta_t + \Delta_N$ for semimetals. In addition to this, spin susceptibility depends on the presence of nodes, which appear as k_0 in Eq. 3.16.

Fig. 3.5 shows that spin susceptibility is linearly proportional to the Fermi energy. As Fermi energy goes away from zero, spin magnetism decreases linearly due to negative sign in Eq. 3.16. Spin susceptibility vanishes for insulating phase which appears when $B = 0.5T$ and $\theta = 80^0$ shown in Fig. 3.5(a) and (b). From the results in Eq. 3.16, we find that spin susceptibility is an oscillatory function of θ. It is seen in Fig. 3.2(d) that nodes disappear in the range $\theta = 78^0$ to $\theta = 102^0$ where the system becomes insulating and χ_s vanishes in the insulating phase. This allows spin susceptibility to be tunable by both Fermi energy and tilt angle of the magnetic field.

In the next section spin-orbit contribution of susceptibility is discussed.

3.3.2 Spin-orbit susceptibility

Spin-orbit susceptibility (χ_{so}) appears due to spin-orbital contribution as given in Eq. 3.13, which on solving for finite temperature gives

$$\chi_{so} = \frac{1}{\beta}\frac{eg\mu_B\cos\theta}{4\pi\hbar}\frac{\partial}{\partial b}\sum_{s,\mu,k_z}\lambda_{s,\mu}\phi[E_{s,\mu}(0)] \tag{3.17}$$

which can be expressed as

$$\chi_{so} \quad = \quad \frac{eg\mu_B\cos^2\theta}{4\pi\hbar}\sum_{s,\mu,k_z} f[E_{s,\mu}(0) - \zeta],$$

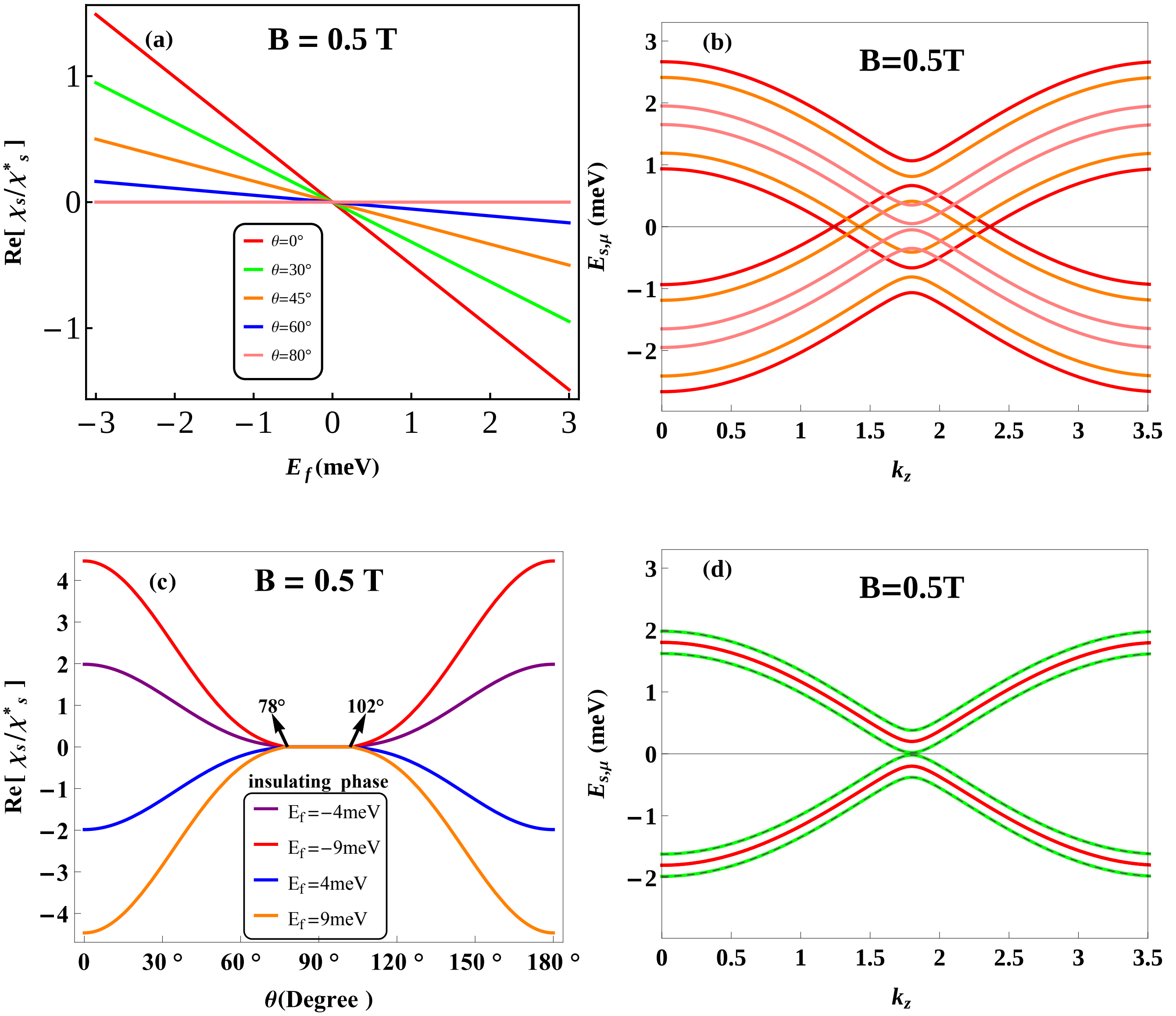

Figure 3.5: Spin susceptibility with (a) Fermi energy in meV and (c) for different orientations of the magnetic field, (b) and (d) show $n = 0$ LLs. Here $\chi_s^* = (\frac{10^2 g\mu_B \cos\theta}{2\hbar v})^2$, $B = 0.5T$, $\Delta_t = 1meV$ and $\Delta_N = 0.8meV$. Colors used in (d) are green for $\theta = 78^0$, red for $\theta = 90^0$ and dotted purple for $\theta = 102^0$.

which for $T \to 0$ becomes

$$\chi_{so} \quad = \quad \frac{eg\mu_B \cos^2\theta}{8\pi^2\hbar} \sum_{s,\mu} \int_{-\infty}^{\infty} dk_z \Theta[E_f - E_{s,\mu}(0)]. \tag{3.18}$$

Above expression shows that χ_{so} is dependent on $n = 0$ energy level branches, both existing and nonexisting, below the Fermi energy. The extra filled LL gives rise to non zero χ_{so}. It is shown in the Fig.3.6 that for semimetallic regime i.e. $\Delta_t - \Delta_N < bcos\theta < \Delta_t + \Delta_N$, χ_{so} is an even function of Fermi energy. In addition to this, there is a change in the behavior of susceptibility when Fermi

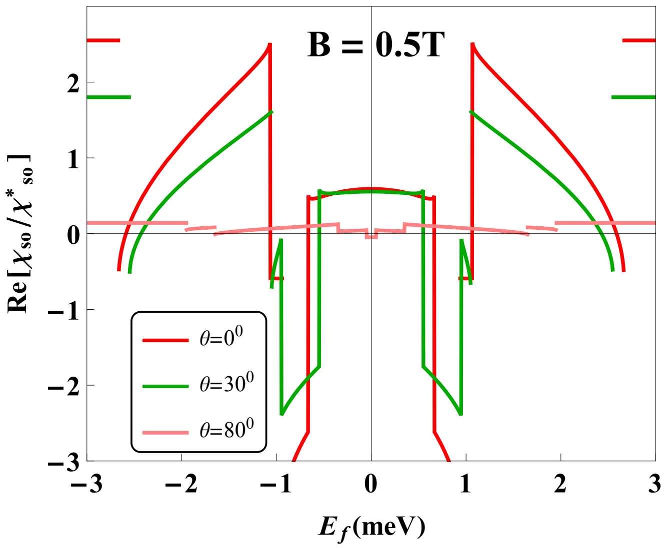

Figure 3.6: Spin-orbit susceptibility with Fermi energy. Here $\chi^*_{so} = \frac{eg\mu_B}{8\pi^2\hbar}$, $B = 0.5T$, $\Delta_t = 1meV$ and $\Delta_N = 0.8meV$.

level moves from one LL to the next. To see this, let us first define zeroth LLs as

$$\begin{aligned} E1(0) &= (bcos\theta - \Delta_D), E2(0) = -(bcos\theta - \Delta_D) \\ E3(0) &= (bcos\theta + \Delta_D), E4(0) = -(bcos\theta + \Delta_D) \end{aligned}$$

Fig. 3.7 shows χ_{so} and the energy spectrum for $n = 0$, when magnetic field is aligned perpendicular to the system. It can be seen that when E_f is below $E4(0)$, χ_{so} is positive and constant due to the bulk contribution of LLs. As $E4(0)$ is approached susceptibility shifts from being negative to positive when E_f is above $E4(0)$. In band gap either between $E4(0)$ and $E1(0)$ or between $E2(0)$ and $E3(0)$, χ_{so} is negative and constant. $E1(0)$ and $E2(0)$ gives negative contribution to susceptibility whereas combined effect of $E1(0)$ and $E2(0)$ about $E_f = 0$ is positive and constant. It can be seen that around the Dirac points χ_{so} is constant, positive and even function of Fermi energy which is also a characteristic of Dirac semimetals[118]. $E3(0)$ contribution to spin orbit susceptibility is from positive to negative. This phase transition also appears when Hall conductivity is measured in topological insulator thin film[117] and graphene[114].

3.3.3 Orbital susceptibility

In this section, we derive the expresson of orbital susceptibility. It is given by Eq. 3.14 which, after some calculation, yields

$$\chi_o = -\frac{e^2 v^2 \cos^2\theta}{6\pi\beta} \sum_{s,\mu,k_z} [\phi'[E_{s,\mu}(0)]. \tag{3.19}$$

Taking derivative of ϕ and executing summation on n we get the expression in terms of Fermi energy $f[E_{s,\mu}(0)]$:

$$\chi_o = -\frac{e^2 v^2 \cos^2\theta}{12\pi} \sum_{s,\mu,k_z} \frac{f[E_{s,\mu}(0)]}{E_{s,\mu}(0)}. \tag{3.20}$$

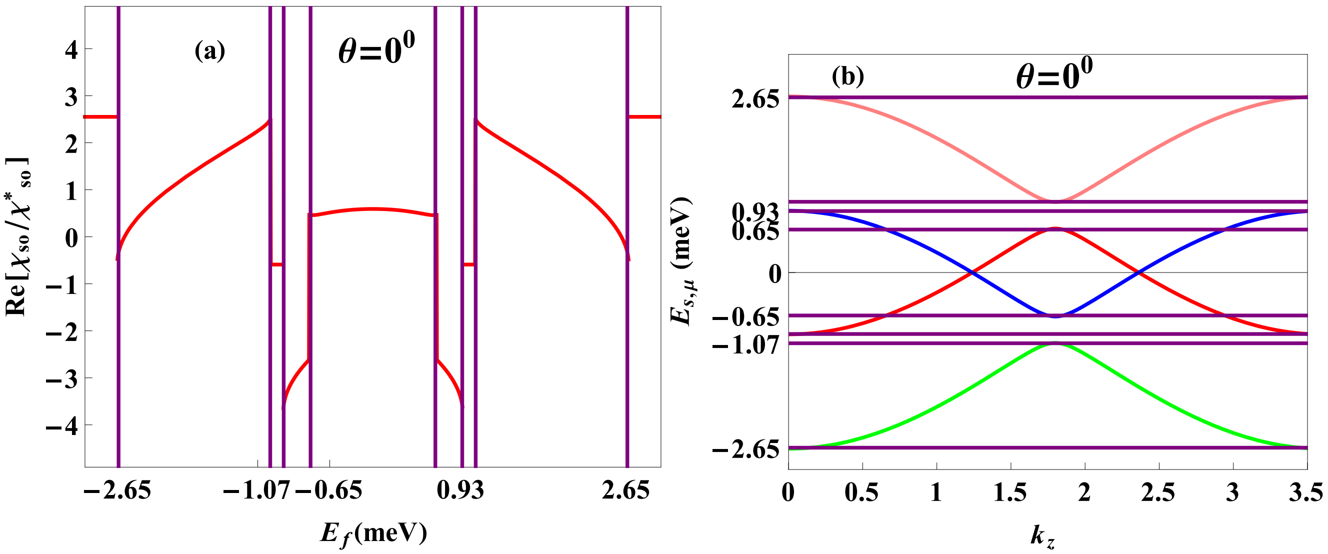

Figure 3.7: (a) Spin-orbit susceptibility with Fermi energy and (b) $n = 0$ LLs. Here $\chi^*_{so} = \frac{eg\mu_B}{8\pi^2\hbar}$, $\Delta_t = 1meV$ and $\Delta_N = 0.8meV$. Colors used are red for $E1(0)$, blue for $E2(0)$, pink for $E3(0)$ and green for $E4(0)$.

For $T \to 0$

$$\chi_o = -\frac{e^2 v^2 \cos^2\theta}{6\pi\beta} \sum_\mu \int_{-\infty}^{\infty} dk_z \frac{\Theta(E_f - E_\mu(0))}{E_\mu(0)}. \tag{3.21}$$

Orbital susceptibility as shown in Fig.(3.8) varies due to the position of Fermi energy with respect to position of zeroth LLs. It can be seen in Fig.(3.8b)that when Fermi energy is such that $E4(0)$ is below it the contribution to χ_o is zero; which remains zero till Fermi energy reaches $E1(0)$ where χ_o becomes diamagnetic. As Fermi level moves towards $E2(0)$ the magnitude of orbital susceptibility is changed but is still diamagnetic till it crosses $E1(0)$. At point node positions χ_o diverges diamagnetically like graphene [112]. From the pure $E2(0)$ LL the contribution to χ_o is positive thus this point appears as phase transition point. When $E3(0)$ comes into play orbital susceptibility starts decreasing but is still positive till it becomes zero when $E3(0)$ is crossed. Orbital susceptibility with angle depicts same contributions of LLs as can be seen in Fig.(3.8d). χ_o is positive due to $E2(0)$ and negative due to $E1(0)$. Due to contribution of $E3(0)$ and $E4(0)$, χ_o starts decreasing till the point comes when at 157.7^0 , χ_o shifts because for $E_f = -1meV$ $E1(0)$ is below the Fermi level and $E4(0)$ is above it and vice versa for $E_f = 1meV$.

3.4 Model for inplane magnetic field

In the previous section, we have presented results for topological semimetals with the magnetic field tilted from $0 \leq \theta < 90^0$ but when magnetic field is oriented at $\theta = 90^0$ Dirac points shift in momentum space. This leads to a new topological phase known as line node semimetal (LNS). For completion we have added magnetic susceptibility for in-plane magnetic field $\theta = 90^0$ which matches the result for single TI thin film[115] when $\Delta_N = 0$. Hamiltonian for the system with the vector potential $\vec{A} = -zB\hat{y}$ in Landau gauge takes the form

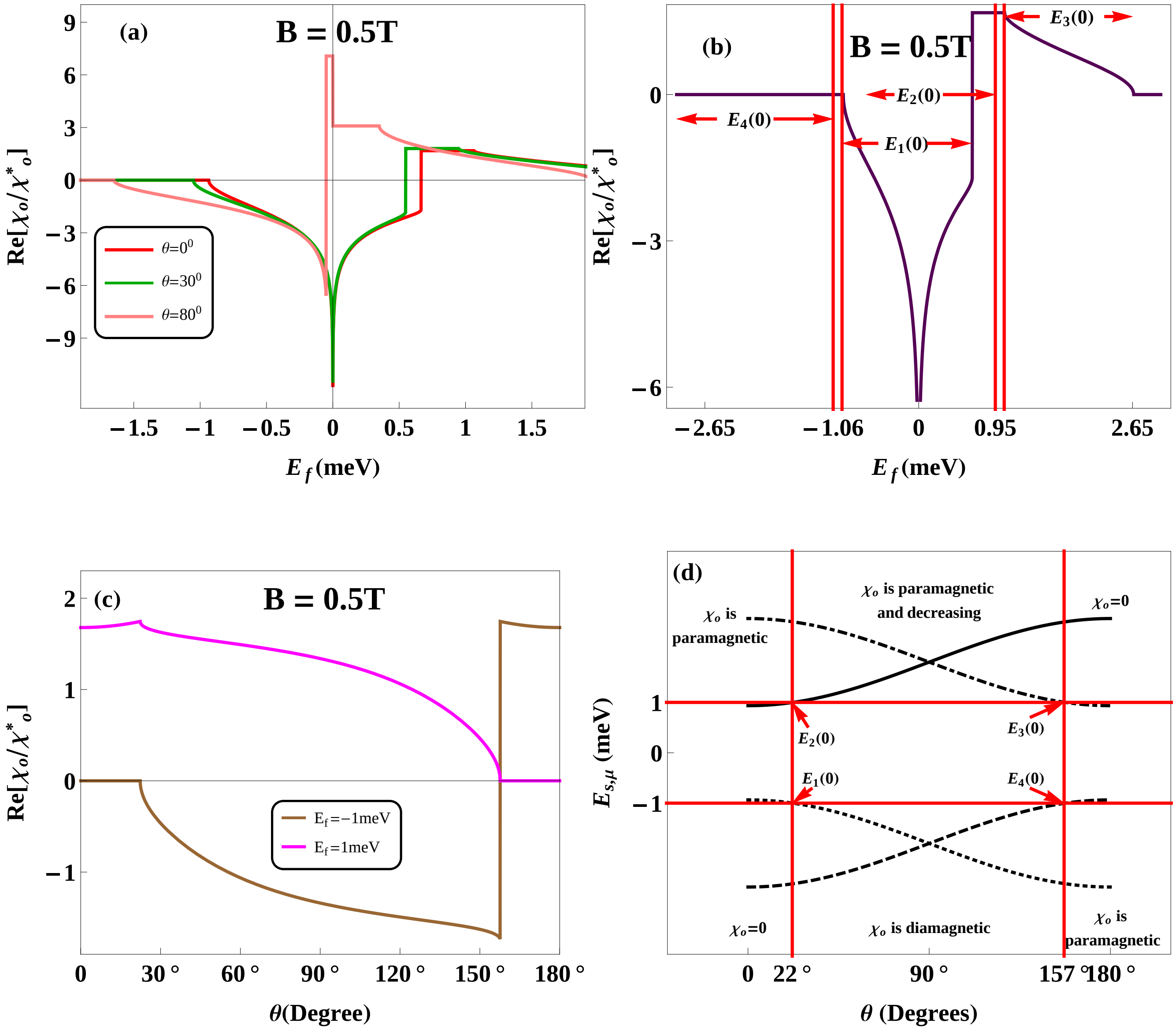

Figure 3.8: Plot of Real component of orbital susceptibility with (a) & (b) Fermi energy in meV and (c) & (d) tilt angle of magnetic field.

$$H_{\|} = \sum_k [v\tau_z(\hat{z}\times\hat{\sigma}).(\hbar\vec{k} - ezB\tau_z\hat{y}) + b\sigma_x + \hat{\Delta}_D(k_z)] \tag{3.22}$$

where $H_{\|}$ is the Hamiltonian for in-plane magnetic field. $b\sigma_x$ is the term arising from Zeeman coupling. To simplify Eq. 3.22 we define $b' = b - vezB$ and the Hamiltonian with corresponding energy become

$$H_{\|} = \sum_k [v\tau_z(-\hbar k_x\sigma_y + \hbar k_y\sigma_x) + b'\sigma_x + \hat{\Delta}_D(k_z)]$$

$H_{\|}$ can be diagnolized to get energy eigen values as

$$E_{k,\pm} = \sqrt{v^2\hbar^2 k_x^2 + (b' \pm \sqrt{v^2\hbar^2 k_y^2 + \Delta_D^2(k_z)})^2}. \tag{3.23}$$

Here $E_{k,\pm}$ is the energy spectrum of the system and $\Delta_D(k_z)$ was defined in Sec. 3.2.
It can be seen in Fig. 3.9 that for $b' < \Delta_t - \Delta_N$ we get insulating state, for $b' = \Delta_t - \Delta_N$ point node appears, when $\Delta_t - \Delta_N < b' < \Delta_t + \Delta_N$ line node appears whereas line node extends to whole BZ when $b' > \Delta_t + \Delta_N$.

3.5 Magnetic susceptibility for in plane magnetic field, $\theta = 90^0$

Magnetic susceptibility is given as

$$\chi = -\frac{\partial^2 F}{\partial B^2} \tag{3.24}$$

$$F = -k_B T \ln[1 + e^{-\beta[E_i(x_n) - \zeta]}]$$

When magnetic field lies in the plane of the material, energy eigenvalue becomes momentum dependent i.e. E_k. The free energy is

$$F = -k_B T \sum_k [\ln(1 + exp^{-\frac{E_{k,\pm} - \zeta}{k_B T}}) + \ln(1 + exp^{\frac{E_{k,\pm} + \zeta}{k_B T}})]. \tag{3.25}$$

Taking Fermi level at zero energy, i.e. $\zeta = 0$ we get

$$\begin{aligned}\frac{\partial F}{\partial B} &= -\sum_k \frac{exp^{\frac{E_{k,+}}{k_B T}}}{1 + exp^{\frac{E_{k,+}}{k_B T}}}(\frac{\partial E_{k,+}}{\partial B}) + \frac{exp^{\frac{E_{k,+}}{k_B T}}}{1 + exp^{-\frac{E_{k,+}}{k_B T}}}(-\frac{\partial E_{k,+}}{\partial B}) \\ &+ \frac{exp^{\frac{E_{k,-}}{k_B T}}}{1 + exp^{\frac{E_{k,-}}{k_B T}}}(\frac{\partial E_{k,-}}{\partial B}) + \frac{exp^{\frac{E_{k,-}}{k_B T}}}{1 + exp^{-\frac{E_{k,-}}{k_B T}}}(-\frac{\partial E_{k,-}}{\partial B}).\end{aligned}$$

To proceed further let us define $\tilde{E}_{k,\pm} = \beta E_{k,\pm}$,where $\beta = \frac{1}{k_B T}$.

$$\begin{aligned}\frac{\partial F}{\partial B} &= -\frac{1}{\beta}\sum_k (\frac{exp^{\tilde{E}_{k,+}}}{1 + exp^{\tilde{E}_{k,+}}} - \frac{exp^{-\tilde{E}_{k,+}}}{1 + exp^{-\tilde{E}_{k,+}}})\frac{\partial \tilde{E}_{k,+}}{\partial B} \\ &+ (\frac{exp^{\tilde{E}_{k,-}}}{1 + exp^{\tilde{E}_{k,-}}} - \frac{exp^{-\tilde{E}_{k,-}}}{1 + exp^{-\tilde{E}_{k,-}}})\frac{\partial \tilde{E}_{k,-}}{\partial B}\end{aligned}$$

$$\frac{\partial F}{\partial B} = -\frac{1}{\beta}\sum_k \frac{\sinh(\tilde{E}_{k,+})}{1 + \cosh(\tilde{E}_{k,+})}\frac{\partial \tilde{E}_{k,+}}{\partial B} + \frac{\sinh(\tilde{E}_{k,-})}{1 + \cosh(\tilde{E}_{k,-})}\frac{\partial \tilde{E}_{k,-}}{\partial B} \tag{3.26}$$

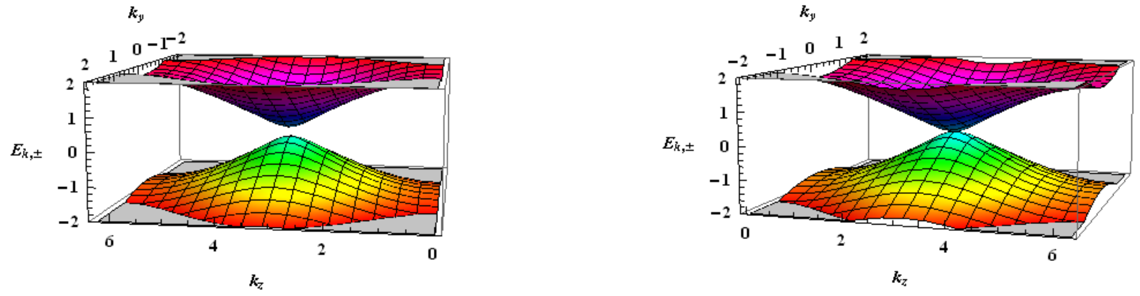

$b' < \Delta_t - \Delta_N$

$b' = \Delta_t - \Delta_N$

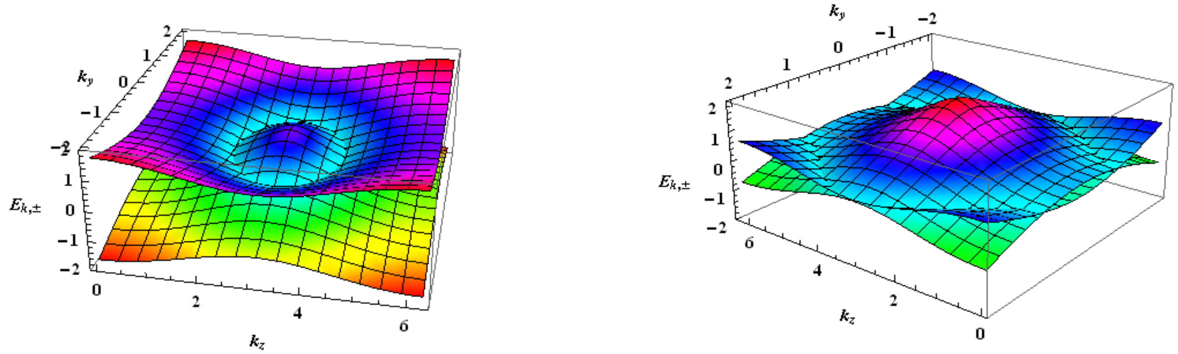

$\Delta_t - \Delta_N < b' < \Delta_t + \Delta_N$

$b' > \Delta_t + \Delta_N$

Figure 3.9: Energy dispersion of line node semimetals for different values of b', $\Delta_t = 1meV$ and $\Delta_N = 0.8meV$.

For $T \to 0$, $\frac{\sinh(\tilde{E}_{k,+})}{1+\cosh(\tilde{E}_{k,+})} \to 1$, therefore Eq. 3.26 on taking second derivative becomes

$$\frac{\partial^2 F}{\partial B^2} \;=\; -\frac{1}{\beta}\sum_k\left(\frac{\partial^2 \tilde{E}_{k,+}}{\partial B^2} + \frac{\partial^2 \tilde{E}_{k,-}}{\partial B^2}\right).$$

From Eq. 3.26, we can write

$$\chi = \frac{1}{\beta}\sum_{k}\left(\frac{\partial^2 \tilde{E}_{k,+}}{\partial B^2} + \frac{\partial^2 \tilde{E}_{k,-}}{\partial B^2}\right). \tag{3.27}$$

For line nodal semimetals we want to calculate magnetic susceptibility χ. In terms of free energy F, the susceptibility χ is given as

$$\chi = -\frac{\partial^2 F}{\partial B^2}$$

To proceed further let us define $\tilde{E}_{k,\pm} = \beta E_{k,\pm}$ and taking Fermi level at zero energy, i.e. $\zeta = 0$ we get

$$\frac{\partial F}{\partial B} = -\sum_{k}\frac{\sinh(\tilde{E}_{k,+})}{1+\cosh(\tilde{E}_{k,+})}\frac{\partial E_{k,+}}{\partial B} + \frac{\sinh(\tilde{E}_{k,-})}{1+\cosh(\tilde{E}_{k,-})}\frac{\partial E_{k,-}}{\partial B}$$

In low temperature regime, $T \rightarrow 0$, $\frac{\sinh(\tilde{E}_{k,+})}{1+\cosh(\tilde{E}_{k,+})} \rightarrow 1$, therefore

$$\frac{\partial^2 F}{\partial B^2} = -\left(\frac{db'}{dB}\right)^2 \int \frac{d^3k}{8\pi^3} v^2\hbar^2 k_x^2\left[\frac{1}{E_{k,+}^3} + \frac{1}{E_{k,-}^3}\right] \tag{3.28}$$

the expression for χ using Eq. 3.28 and the approximation $\Delta_D(k_z) \approx (\Delta_t + \Delta_N)^2 - \Delta_t\Delta_N k_z^2$, becomes

$$\chi = -\left(\frac{g\mu_B}{2} - vez\right)^2 \frac{(\Delta_t + \Delta_N)^2 - b'^2}{4\pi v^2\sqrt{\Delta_t\Delta_N}} \tag{3.29}$$

which is the required expression for susceptibility. It must be noted that in the insulating phase

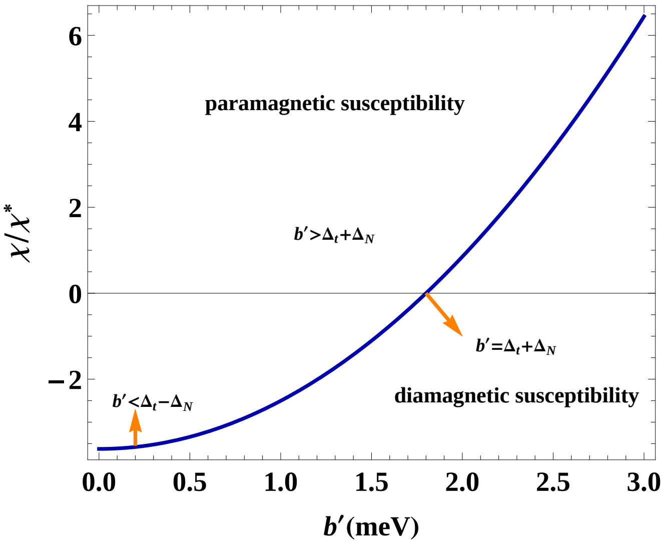

Figure 3.10: Magnetic susceptibility of line node semimetals with b', $\Delta_t = 1meV$ and $\Delta_N = 0.8meV$.

$(b' < \Delta_t - \Delta_N)$ when the gap is opened by strong hybridization, we get diamagnetic response which vanishes when $b' = \Delta_t + \Delta_N$. Thus for LNS we have diamagnetic response but for the case when nodal line extends to entire BZ, there is a shift in the susceptibility from paramagnetic to diamagnetic as shown in Fig.3.10.

3.6 Results

In this chapter, magnetic susceptibility of Weyl semimetals, placed in a tilted magnetic field, was studied. We find three contributions to susceptibility: spin, orbital and spin-orbital; all three contributions are investigated for a tilted magnetic field. We find that spin susceptibility at low temperature varies linearly with Fermi energy and is oscillatory function of tilt angle; orbital contribution shows diamagnetic divergence at zero Fermi energy similar to graphene and spin orbital contribution is an even function of Fermi energy and tilt angle. Due to anisotropic nature of magnetic response, we propose that spin, orbital and spin-orbital magnetic response can be distinguished by changing the orientation of the applied magnetic field. It can be seen from the discussion of tilted magnetic field and in plane magnetic field that application of tilted magnetic field helps us to identify all the contributions of susceptibility whereas it is not possible for the application of in plane magnetic field.

Chapter 4

Far from equilibrium Response of Semi-Dirac Materials to Broken Time Reversal Symmetry

4.1 Introduction

In this chapter, we study far from equilibrium response with emphasis on TRS. Dirac materials as previously discussed are materials with low energy excitations which behave like Dirac fermions with relativistic dispersion. They can be bulk gapped or semimetallic. A class of Dirac materials are those which show linear dispersion along one direction and quadratic dispersion along the perpendicular direction, they are known as semi-Dirac materials. They have been studied theoretically in three unit cell TiO_2/V_2O_3 [119, 120], using group theory[121] and have been found exerimentally in $\alpha-(BEDTTF)213$ salt[122]. They have also been proposed in graphene like models with tunable hopping parameters which gives rise to semi-Dirac phase[123, 124]. They can also be created in cold atoms and merging of Dirac points have been experimentally seen in fermionic cold atoms [125]. The unique hybrid dispersion makes them anisotropic with interesting properties [126, 127, 128, 129, 130, 131, 132, 133, 134, 136, 137, 135, 138]

A quench protocol is implemented to study the far from equilibrium response. A system is prepared in the ground state of the Hamiltonian that depends on a parameter that is changed abruptly. This is known as quenching the system. The quenched state is allowed to evolve and its response is studied. This procedure creates far equilibrium states whose response is studied here.

In this chapter we investigate the far from equilibrium response of semi-Dirac materials which are exposed to light. A unique result is found which is different from its equilibrium analog. We show that there is Hall current in the system even with TRS whereas in the equilibrium case Hall current exists only when TRS is broken. This postquench effect is unique in many aspects and it can be understood while considering precession of the spinor on Bloch sphere which shifts the center of rotation on the application of pulse[139]. Ultracold atoms are found to be potential candidates for the observation of interacting condensed systems and their topological properties give insight to out of equilibrium behaviors for bosonic and fermionic systems[140, 141, 142, 143].

4.2 Model for semi-Dirac materials

We consider semi-Dirac materials as our model system with nonrelativistic dispersion along the x-axis and relativistic dispersion along the y-axis. Two dimensional low energy semi-Dirac materials are described by the Hamiltonian[144]

$$H_0(\mathbf{k}) = (\frac{k_x^2}{m^*} - \Delta_0)\tau_x + vk_y\tau_y \tag{4.1}$$

where m^* is quasiparticle mass, τ_i are the Pauli matrices in pseudospin space, Δ_0 is the tunable band gap in the energy spectrum, k_x, k_y are the momentum along x and y-axis respectively and v is Dirac velocity. It can be seen that the Hamiltonian in Eq. (4.1) is invariant under time reversal. Diagonalizing the Hamiltonian gives the energy spectrum

$$E_0(k) = s\sqrt{(\frac{k_x^2}{m^*} - \Delta_0)^2 + (vk_y)^2}$$

where $s = \pm$ for conduction and valence bands.

As shown in Fig. 4.1 when $\Delta_0 < 0$ we have an insulating phase, for $\Delta_0 = 0$ we have linear spectrum and for $\Delta_0 > 0$ we have two Dirac points.

To start with we photoinduce the system with monochromatic light field strength A_0, frequency ω and polarization angle ϕ. Here we have considered only time dependence and neglected the spatial dependence of electromagnetic field by considering the fact that sample size is small as compared to the wavelength. The light couples to the system and make the defining Hamiltonian given in Eq. (4.1) time dependent. In the presence of light Eq. (4.1) becomes $H_0(\mathbf{k}, t) = H_0(\mathbf{k}) + H_1(\mathbf{k}, t)\sigma_x + H_2(\mathbf{k}, t)\sigma_y$. This time dependent Hamiltonian is solved using Floquet formalism. Floquet Hamiltonian is expressed up to first order $H_F(\mathbf{k}, m_{ef}) \approx H_F(\mathbf{k})^0 + H_F(\mathbf{k})^1$. Here $H_F(\mathbf{k})^0 = H_0(\mathbf{k}) + \frac{e^2A_0^2}{2m^*}\tau_x$ and gap opening term $H_F(\mathbf{k})^1 = m_0 + \beta k_x^2 + \gamma k_x + \eta k_x k_y$ is momentum dependent. Eq. 4.1 can be expreseed as[144]

$$H_F(\mathbf{k}, m_{ef}) = \mathbf{h}(\mathbf{k}).\tau \tag{4.2}$$

where H_F is the Floquet Hamiltonian, $\mathbf{h}(\mathbf{k}) = (\frac{k_x^2}{m^*} + \Delta_1, vk_y, m_{ef})$, $\Delta_1 = \frac{e^2A_0^2}{2m^*} - \Delta_0$, $m_{ef} = m_0 + \beta k_x^2 + \gamma k_x + \eta k_x k_y$, $m_0 = \frac{veA_0cos\phi}{\hbar\omega}(\frac{e^2A_0^2}{m^*} - 2\Delta_0)$, $\beta = \frac{2veA_0cos\phi}{\hbar\omega m^*}$, $\gamma = \frac{2ve^2A_0^2sin\phi}{\hbar\omega m^*}$ and $\eta = -\frac{4veA_0}{\hbar\omega m^*}$. We can see that the m_{ef} term in the Hamiltonian breaks TRS.

The energy spectrum of the Floquet Hamiltonian is given by

$$E_F(k, m_{ef}) = s\sqrt{(\frac{k_x^2}{m^*} + \Delta_1)^2 + (vk_y)^2 + m_{ef}^2}. \tag{4.3}$$

To simplify the calculation and focus on Hall response we restrict our study to circularly polarized light ($\phi = \pm\pi/2$). We obtain results that depend on the value of Δ_0. As shown in Fig.(2), when $\Delta_0 < \frac{e^2A_0^2}{2m^*}$ there is the trivial insulating phase, for $\Delta_0 = \frac{e^2A_0^2}{2m^*}$ spectrum becomes gapless and for $\Delta_0 > \frac{e^2A_0^2}{2m^*}$ Dirac nodes shift their position relative to the case when no light was shining on the system and the system is described by Eq.(4.1).

We proceed to determine the Hall response in the next section.

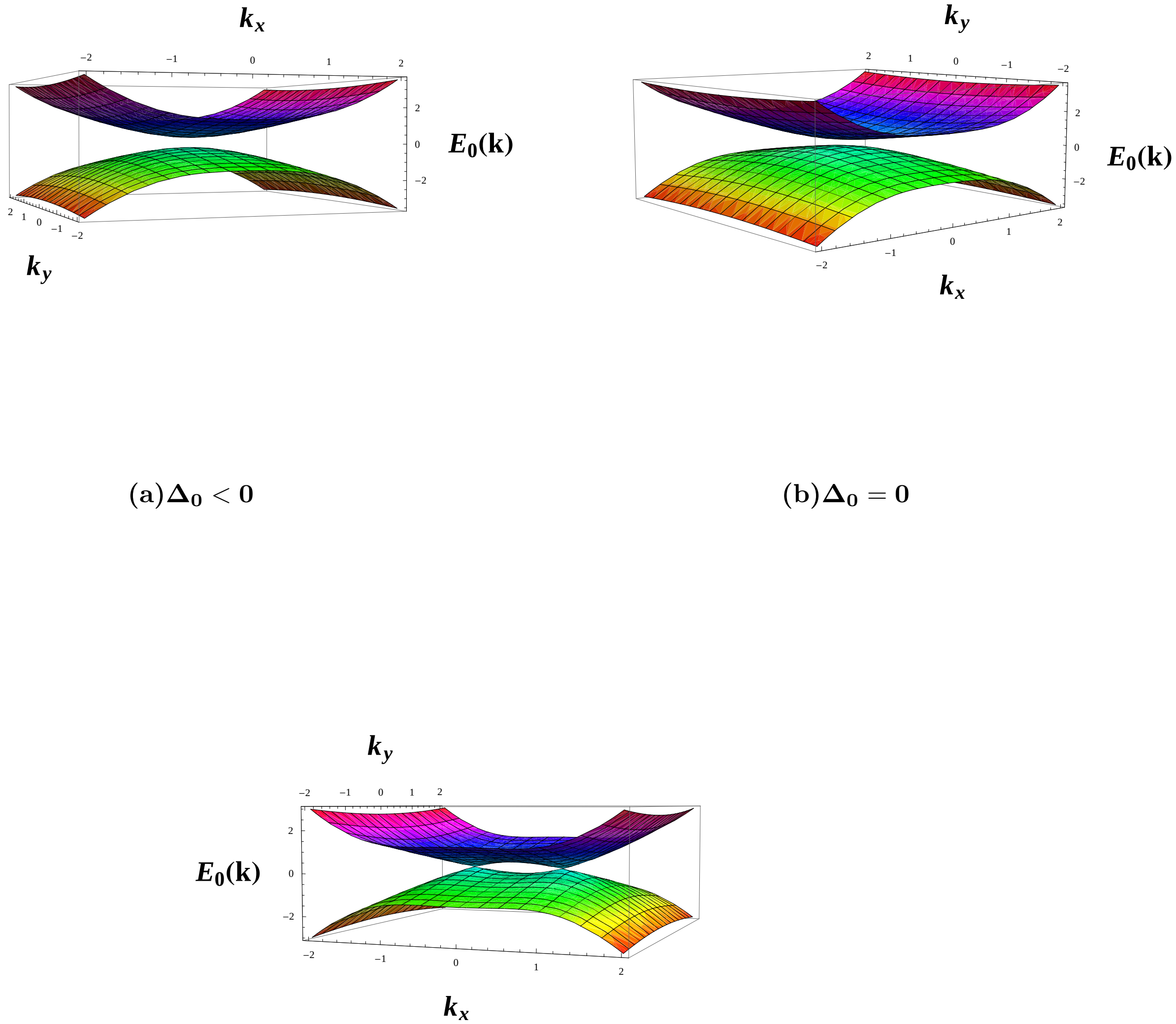

(a)$\mathbf{\Delta_0 < 0}$

(b)$\mathbf{\Delta_0 = 0}$

(c)$\mathbf{\Delta_0 > 0}$

Figure 4.1: Energy spectrum of semi-Dirac materials obtained from the Hamiltonian in Eq.(4.1). Spectrum (a) is a typical insulating phase, (b) is linear along k_y and (c) has two Dirac points. Here $v = 0.65 eV\mathring{A}$, $\frac{1}{m^*} = 0.75 eV\mathring{A}^2$.

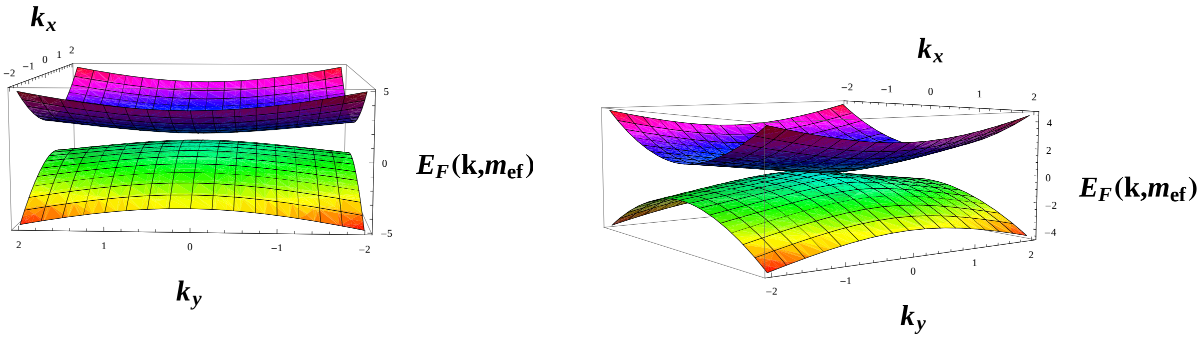

(a) $\mathbf{\Delta_0 < \frac{e^2A_0^2}{2m^*}}$ **(b)** $\mathbf{\Delta_0 = \frac{e^2A_0^2}{2m^*}}$

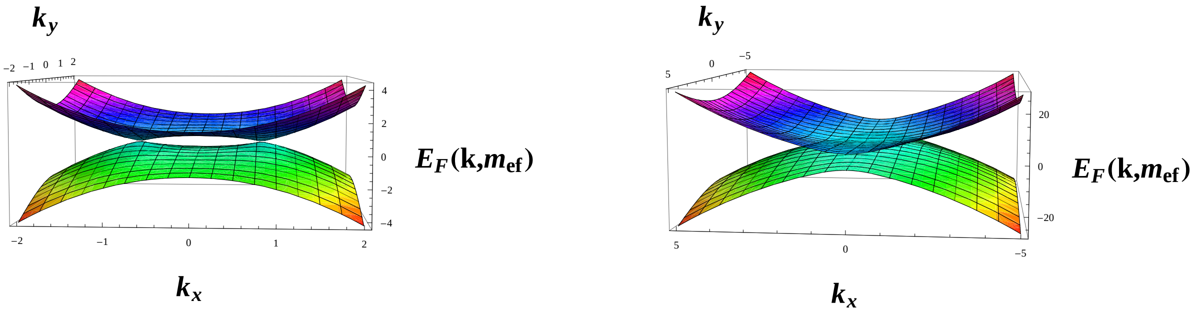

(c) $\mathbf{\Delta_0 > \frac{e^2A_0^2}{2m^*}}$ **(d)** $\mathbf{\Delta_0 = 0}$

Figure 4.2: Energy spectrum of photoinduced (circularly polarized) semi-Dirac materials obtained from the Hamiltonian in Eq.(4.2) (a) for insulating phase, (b) gapless state and (c) shifted Dirac cones. Here $v = 0.65 eV\mathring{A}$, $\frac{1}{m^*} = 0.75 eV\mathring{A}^2$, $\phi = \pi/2$, $eA_0 = 0.1\mathring{A}^{-1}$.

4.3 Hall Response of semi-Dirac materials

To study the Hall response of far equilibrium states in semi-Dirac materials, we proceed with the following protocol:
A. We begin with the system in an initial eigen state $|\Psi_0\rangle$ of the Floquet Hamiltonian $H_F(\mathbf{k}, m_{ef})$.
B. At time $t = 0$, quenching of $H_F(\mathbf{k}, m_{ef})$ is done by taking $m_{ef} = 0$.
C. The state $|\Psi_0\rangle$ is time evolved to t_1 using time evolution operator $e^{-it_1 H_{F,0}(\mathbf{k},0)}$ such that the time evolved state at t_1 is $|\Psi_1\rangle$.
D. The state $|\Psi_1\rangle$ is pulsed at time t_1.
E. At $t = t_2$, the pulsed state $|\Psi_1\rangle$ is then time evolved using time evolution operator $e^{-i(t_2-t_1)H'_F(\mathbf{k},\mathbf{0})}$ to state $|\Psi_2\rangle$.
F. Hall response is studied for the state $|\Psi_2\rangle$ at time t_2.

Let us formally go through the steps mentioned above:

4.3.1 Preparation of initial state

The spinor state of our semi-Dirac system which has been exposed to light, under high frequency expansion[144] of Floquet Hamiltonian Eq.4.2, can be written in terms of up spin $|\uparrow\rangle \equiv \begin{pmatrix}1\\0\end{pmatrix}$ and down spin $|\downarrow\rangle \equiv \begin{pmatrix}0\\1\end{pmatrix}$ states as

$$|\Psi_0\rangle = cos(\theta/2)|\uparrow\rangle - e^{i\Phi} sin(\theta/2)|\downarrow\rangle \tag{4.4}$$

which can be conveniently written as

$$|\Psi_0\rangle = \begin{pmatrix} cos(\theta/2) \\ e^{i\Phi} sin(\theta/2) \end{pmatrix}$$

where $e^{i\Phi} = \frac{(\frac{k_x^2}{m^*}+\Delta_1)+i(vk_y)}{\sqrt{E_F^2(k,m_{ef})-m_{ef}^2}}$, $cos\theta = \frac{m_{ef}}{E_F(k,m_{ef})}$, $sin\theta = \frac{\sqrt{E_F^2(k,m_{ef})-m_{ef}^2}}{E_F(k,m_{ef})}$ and
$E_F(k, m_{ef}) = s\sqrt{(\frac{k_x^2}{m^*} + \Delta_1)^2 + (vk_y)^2 + m_{ef}^2}$.

To proceed further, we quench the mass parameter m_{ef} in Hamiltonian, $H_F(\mathbf{k}, m_{ef})$ given in Eq.(4.2). By removing the term in the Hamiltonian which explicitly breaks TRS, the Hamiltonian becomes invariant under time-reversal.

4.3.2 Parameter Quenching

At time $t = 0$, we quench $H_{F,0}(\mathbf{k}, m_{ef}) \rightarrow H_{F,0}(\mathbf{k}, 0)$. For this we switch off the incident light, given as A_0 in the expression of m_{ef}, which will make the coefficients β, γ and η and m_0 vanish. Therefore $H_{F,0}(\mathbf{k}, 0)$ can be written as

$$H_{F,0}(\mathbf{k}, 0) = \mathbf{h_0}(\mathbf{k}).\sigma \tag{4.5}$$

where $\mathbf{h_0}(\mathbf{k}) = (\frac{k_x^2}{m^*} + \Delta_1, vk_y, 0)$.
The explicit form of the Hamiltonian is

$$H_{F,0}(\mathbf{k}, 0) = \begin{pmatrix} 0 & \frac{k_x^2}{m^*} + \Delta_1 - ivk_y \\ \frac{k_x^2}{m^*} + \Delta_1 + ivk_y & 0 \end{pmatrix}$$

This is the quenched Hamiltonian obtained by switching off the incident light falling on the system. The time evolution of the quenched state will be discussed next.

4.3.3 Time evolution of quenched state

The quenched state is time evolved by applying the time evolution operator on the state. The time evolution operator can be expressed as a 2x2 matrix. The 2x2 time evolution operator is

$$\begin{aligned} e^{-it_1 H_{F,0}(\mathbf{k},0)} &\equiv e^{-it_1 \mathbf{h_0}(\mathbf{k}).\sigma} \\ &= cos(h_0 t_1) - isin(h_0 t_1)(\frac{\mathbf{h_0}.\sigma}{|h_0|}) \end{aligned} \tag{4.6}$$

where

$$\begin{aligned} |h_0| &= s\sqrt{(\frac{k_x^2}{m^*} + \Delta_1)^2 + (vk_y)^2} \\ &= s\sqrt{E_F^2(k, m_{ef}) - m_{ef}^2}. \end{aligned}$$

The time evolution operator can be expressed as

$$\begin{aligned} e^{-it_1 H_{F,0}(\mathbf{k},0)} &= \begin{pmatrix} cos(h_0 t_1) & 0 \\ 0 & cos(h_0 t_1) \end{pmatrix} - i\frac{sin(h_0 t_1)}{|h_0|} \begin{pmatrix} 0 & \frac{k_x^2}{m^*} + \Delta_1 - ivk_y \\ \frac{k_x^2}{m^*} + \Delta_1 + ivk_y & 0 \end{pmatrix} \\ &= \begin{pmatrix} cos(h_0 t_1) & -isin(h_0 t_1)e^{-i\Phi} \\ -isin(h_0 t_1)e^{i\Phi} & cos(h_0 t_1) \end{pmatrix}. \end{aligned}$$

Now we apply the time evolution operator to the initial state to get the state $|\Psi_1\rangle$ at later time t_1:

$$\begin{aligned} |\Psi_1\rangle &= e^{-it_1 H_{F,0}(\mathbf{k},0)}|\Psi_0\rangle \\ &= \begin{pmatrix} cos(h_0 t_1) & -isin(h_0 t_1)e^{-i\Phi} \\ -isin(h_0 t_1)e^{i\Phi} & cos(h_0 t_1)) \end{pmatrix} \begin{pmatrix} cos(\theta/2) \\ -e^{i\Phi} sin(\theta/2) \end{pmatrix} \\ &= \begin{pmatrix} cos(h_0 t_1)cos(\theta/2) + isin(h_0 t_1)sin(\theta/2) \\ (-isin(h_0 t_1)cos(\theta/2) - cos(h_0 t_1)sin(\theta/2))e^{i\Phi} \end{pmatrix} \end{aligned}$$

which in terms of $\{|\uparrow\rangle, |\downarrow\rangle\}$ can be written as

$$|\Psi_1\rangle = a(t_1)|\uparrow\rangle - e^{i\Phi} b(t_1)|\downarrow\rangle \tag{4.7}$$

where $a(t_1) = cos(h_0 t_1)cos(\theta/2) + isin(h_0 t_1)sin(\theta/2)$
and $b(t_1) = isin(h_0 t_1)cos(\theta/2) + cos(h_0 t_1)sin(\theta/2)$.

The time evolved state will be pulsed now, this is discussed in the next section.

4.3.4 Pulsing the state

To pulse the state $|\Psi_1\rangle$, we use minimal coupling, i.e substituting $\mathbf{k} \to \mathbf{k} - \mathbf{eA}$. In order to simplify calculations we assume that $\frac{e|\mathbf{A}|}{\mathbf{h_0}(\mathbf{k})} << 1$. Following this assumption higher order terms $O(A^2)$ can be neglected.

We can see that the phase angle Φ is now shifted to Φ_A and let us call this shift $\Delta\Phi = \Phi_A - \Phi$. Then we can write $|h'|$

$$\begin{aligned}
|h'| &= \sqrt{(\frac{(k_x - eA_x)(k_x - eA_x)}{m^*} + \Delta_1)^2 + (vk_y)^2} \\
&= \sqrt{(\frac{(k_x^2 - e(A_xk_x + k_xA_x)}{m^*} + \Delta_1)^2 + (vk_y)^2} \\
&= \sqrt{(\frac{k_x^2}{m^*} + \Delta_1)^2 + (vk_y)^2 - 2\frac{e(A_xk_x + k_xA_x)(\frac{k_x^2}{m^*} + \Delta_1)}{m^*}} \\
&= \sqrt{(|h_0|)^2 - 2e|h_0|cos\Phi\frac{(A_xk_x + k_xA_x)}{m^*}} \\
&= |h_0| - ecos\Phi\frac{(A_xk_x + k_xA_x)}{m^*}. \qquad (4.8)
\end{aligned}$$

We will need $e^{i\Delta\Phi}$ in subsequent calculations, therefore we simplify its expression

$$\begin{aligned}
e^{i\Delta\Phi} &= \frac{e^{i\Phi_A}}{e^{i\Phi}} \\
&= \frac{\frac{(k_x^2 - e(A_xk_x + k_xA_x)}{m^*} + \Delta_1 + ivk_y}{\frac{k_x^2}{m^*} + \Delta_1 + ivk_y} \\
&= 1 - \frac{e|h_0|cos\Phi}{m^*}\frac{A_xk_x + k_xA_x}{|h_0|^2} + i\frac{e|h_0|sin\Phi}{m^*}\frac{A_xk_x + k_xA_x}{|h_0|^2} \\
&= \frac{|h'|}{|h_0|} + i\frac{esin\Phi}{m^*}\frac{A_xk_x + k_xA_x}{|h_0|} \\
e^{i\Delta\Phi} &= 1 + i\frac{esin\Phi}{m^*}\frac{A_xk_x + k_xA_x}{|h_0|} \qquad (4.9)
\end{aligned}$$

After pulsing the state we time evolve the state $|\Psi_1\rangle$ which is presented next.

4.3.5 Time evolution of pulsed state.

The state $|\Psi_1\rangle$ pulsed at $t = t_1$ is now time evolved to later time $t = t_2$ using time evolution operator $e^{-i(t_2-t_1)H'_F(\mathbf{k},\mathbf{0})}$ as defined in Eq.(4.6). Explicitly it is

$$e^{-i\delta_t H'_F(\mathbf{k},\mathbf{0})} = \begin{pmatrix} cos[h'\delta_t] & -isin[h'\delta_t]e^{-i\Phi_A} \\ -isin[h'\delta_t]e^{i\Phi_A} & cos[h'\delta_t] \end{pmatrix}$$

where $e^{i\Phi_A} = \frac{k_x^2 - e(A_xk_x + k_xA_x)}{m^*} + \Delta_1 + ivk_y$, $\delta_t = t_2 - t_1$ and h' is defined in Eq. 4.8.

To obtain state $|\Psi_2\rangle$ at $t = t_2$,we have

$$\begin{aligned}
|\Psi_2\rangle &= e^{-i\delta_t H'_F(\mathbf{k},\mathbf{0})}|\Psi_1\rangle \\
&= \begin{pmatrix} cos[h'\delta_t] & -isin[h'\delta_t]e^{-i\Phi_A} \\ -isin[h'\delta_t]e^{i\Phi_A} & cos[h'\delta_t] \end{pmatrix}\begin{pmatrix} a(t_1) \\ -e^{i\Phi}b(t_1) \end{pmatrix} \\
&= \begin{pmatrix} cos[h'\delta_t]a(t_1) + isin[h'\delta_t]e^{-i(\Phi_A-\Phi)} \\ -isin[h'\delta_t]e^{i\Phi_A} - cos[h'\delta_t]e^{i\Phi} \end{pmatrix}.
\end{aligned}$$

Lastly, we want to determine the Hall response. Since the pulse is applied in the x-direction, the current in the y-direction is the Hall current that we determine next.

4.3.6 Hall response

To determine Hall response along y-direction we need to calculate average of σ_y in state $|\Psi_2\rangle$. To obtain the answer we use the following mathematical identity:

$$\begin{aligned} \langle\Psi_i|\sigma_y|\Psi_i\rangle &= \frac{1}{i}(\sigma^+ - \sigma^-) \\ &= 2Im(\langle\sigma^+\rangle). \end{aligned} \tag{4.10}$$

We also note that

$$\sigma_y = \frac{1}{i}(\sigma^+ - \sigma^-)$$

Since

$$\begin{aligned} \sigma_y(t) = U^\dagger(t)\sigma_y U(t) \\ &= \sigma_y(t) = \frac{1}{i}(\sigma^+(t) - \sigma^-(t)) \end{aligned}$$

Therefore we can write J_y as

$$-e\langle\Psi_2|\sigma_y|\Psi_2\rangle = -2eIm(\langle\Psi_1|(e^{-i\delta_t H'_F(\mathbf{k},\mathbf{0})})^\dagger\sigma^+ e^{-i\delta_t H'_F(\mathbf{k},\mathbf{0})}|\Psi_1\rangle).$$

As

$$\begin{aligned} &(e^{-i\delta_t H'_F(\mathbf{k},\mathbf{0})})^\dagger\sigma^+ e^{-i\delta_t H'_F(\mathbf{k},\mathbf{0})} \\ = &\begin{pmatrix} \\ cos[h'\delta_t] & isin[h'\delta_t]e^{-i\Phi_A} \\ isin[h'\delta_t]e^{i\Phi_A} & cos[h'\delta_t] \end{pmatrix} \quad \begin{pmatrix} -isin[h'\delta_t]e^{-i\Phi_A} & cos[h'\delta_t] \\ 0 & 0 \end{pmatrix} \\ = &\begin{pmatrix} -\frac{i}{2}sin[h'\delta_t]e^{i\Phi_A} & cos^2[h'\delta_t] \\ sin^2[h'\delta_t]e^{2i\Phi_A} & \frac{i}{2}sin[h'\delta_t]e^{i\Phi_A} \end{pmatrix}. \end{aligned}$$

Therefore using Eq. 4.7 we have

$$\begin{aligned} J_y &= -2eIm[\begin{pmatrix} a^*(t_1) & -e^{-i\Phi}b^*(t_1) \end{pmatrix} * \begin{pmatrix} -\frac{i}{2}sin[2h'\delta_t]e^{i\Phi_A} & cos^2[h'^{\delta_t}] \\ sin^2[h'\delta_t]e^{2i\Phi_A} & \frac{i}{2}sin[2h'\delta_t]e^{i\Phi_A} \end{pmatrix}\begin{pmatrix} a(t_1) \\ -e^{i\Phi}b(t_1) \end{pmatrix}] \\ &= -2eIm[\begin{pmatrix} a^*(t_1) & -e^{-i\Phi}b^*(t_1) \end{pmatrix} * \begin{pmatrix} -\frac{ia(t_1)}{2}sin[2h'\delta_t]e^{i\Phi_A} - \frac{1+cos[2h'\delta_t]}{2}e^{-i\Phi}b^*(t_1) \\ \frac{1+cos[2h'\delta_t]}{2}e^{2i\Phi_A}a(t_1) - \frac{ie^{-i\Phi}b^*(t_1)}{2}sin[2h'\delta_t]e^{i\Phi_A} \end{pmatrix}] \end{aligned}$$

which can be written as

$$\begin{aligned} J_y = -eIm[e^{i\Phi}\{-i \quad &(|a|^2 - |b|^2)e^{i\Delta\Phi}sin[2h'\delta_t] \\ - \quad ab^*e^{2i\Delta\Phi}(1 - cos[2h'\delta_t]) \quad &-a^*b(1 + cos[2h'\delta_t])\}] \end{aligned} \tag{4.11}$$

where

$$\begin{aligned} |a|^2 - |b|^2 &= cos\theta cos[2h_0t_1] \\ ab^* &= \frac{1}{2}(-icos\theta sin[2h_0t_1] + sin\theta) \\ a^*b &= \frac{1}{2}(icos\theta sin[2h_0t_1] + sin\theta) \end{aligned}$$

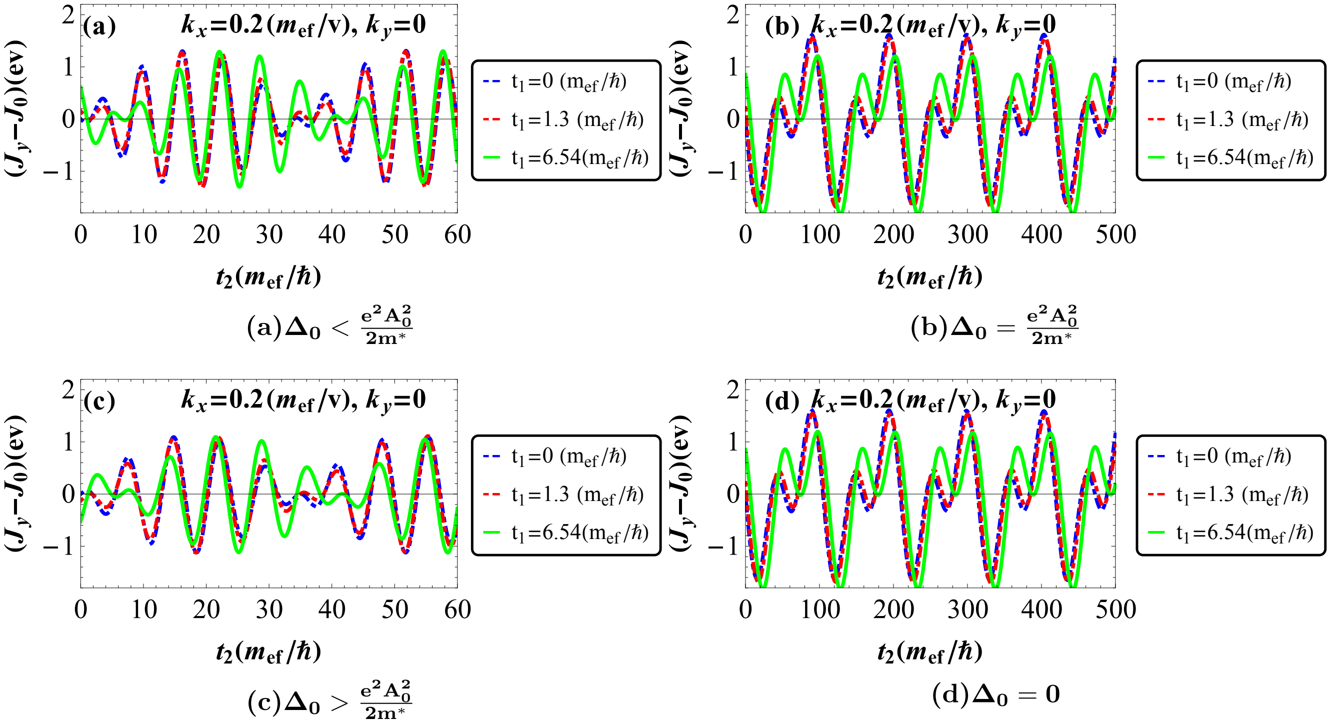

(a)$\boldsymbol{\Delta_0 < \frac{e^2A_0^2}{2m^*}}$ (b)$\boldsymbol{\Delta_0 = \frac{e^2A_0^2}{2m^*}}$

(c)$\boldsymbol{\Delta_0 > \frac{e^2A_0^2}{2m^*}}$ (d)$\boldsymbol{\Delta_0 = 0}$

Figure 4.3: Current response of a single state when $\Phi = 0$, $eA = 0.3\mathring{A}^{-1}$.

and h' is defined in Eq. 4.8.

This shows that a non zero Hall response for our system is found even when the Hamiltonian does not break instantaneous TRS. The condition required to get this response is to break TRS or mirror symmetry either before quenching or after it. In Fig. 4.3, we have plotted $J_y - J_y|_{A\to 0}$ for a single state to compare it with the non-pulsed current at $\Phi = 0$.

We find that remnant Hall current appears in semi-Dirac materials when the system is in the insulating or nodal phase. Hall current is oscillatory and beating phenomenon having a specific frquency is seen for the insulating phase and also when Dirac cones appear as shown in Figs. 4.3(a) and (c). The oscillations appear for the other two cases but they donot have a specific frequency for a semi-Dirac state. We can see that the center of oscillation gets shifted when momentum and pulse are perpendicular as shown in Fig. 4.4. Beating pattern arises because of the interference of the pulsed and non-pulsed current. When the pulse is in phase $\Phi = 0$ and it goes away for $\Phi = \Pi/2$, (out of phase) and moementum are in the same direction. There is same behavior for insulating and Dirac phase for both directions of pulse.

Previously we calculated the Hall response for a single state, to obtain the contribution from all the states we determine the current for states around a ring of fixed momentum:

$$J_{Hall} = -e\int_0^{2\pi} \frac{1}{2\pi}\langle\Psi_2|\sigma_y|\Psi_2\rangle d\phi.$$

On carrying out the integration we get

$$J_{Hall} = -\frac{ecos\theta}{h_0}[\mathbf{J_1}[X]\{\frac{sin2h_0t_2}{(t_1-t_2)} - cos2h_0t_2\} - \frac{Ak_x}{m^*}sin2h_0t_1]. \tag{4.12}$$

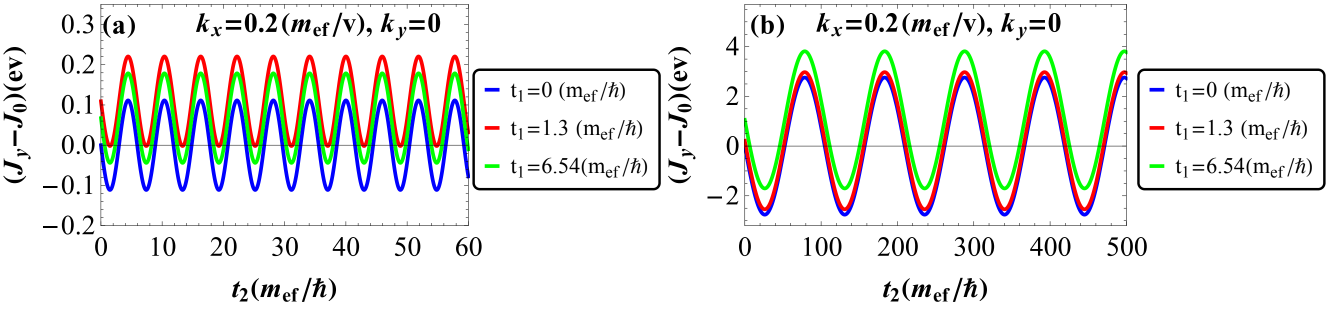

(a)$\mathbf{\Delta_0 < \frac{e^2A_0^2}{2m^*}}$ (b)$\mathbf{\Delta_0 = \frac{e^2A_0^2}{2m^*}}$

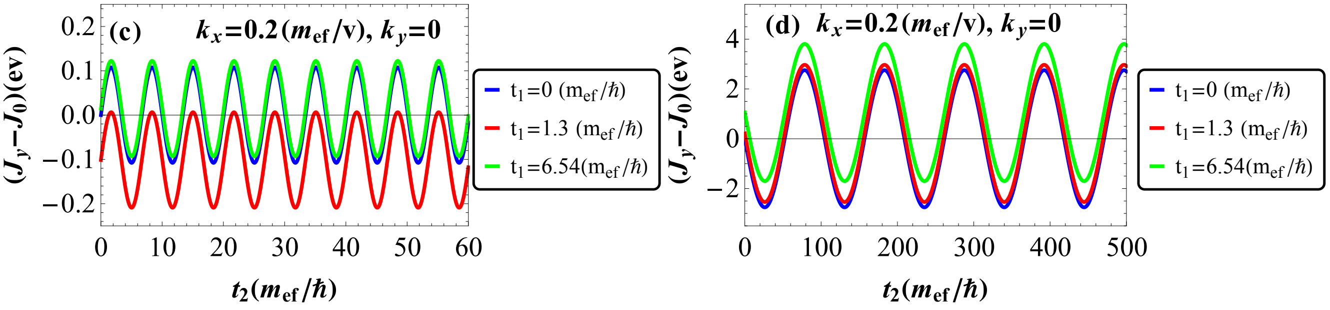

(c)$\mathbf{\Delta_0 > \frac{e^2A_0^2}{2m^*}}$ (d)$\mathbf{\Delta_0 = 0}$

Figure 4.4: Current response of single state when $\Phi = \Pi/2$, $eA = 0.3\mathring{A}^{-1}$.

Here $X = \frac{4Ak_x(t_1-t_2)}{2m^*}$. Since the Bessel function $\mathbf{J_1}$ in Eq. 4.12 depends on k_x, J_{Hall} exhibits oscillation in k_x. And $\mathbf{J_1}$ dies off for longer times i.e. when $t_2 \to \infty$.Eq. 4.12 has been plotted in Fig.4.5 and 4.6. It can be seen in Fig. 4.5 that in the phases which corresponds to different values of Δ_0, J_{Hall} is oscillatory, though it decays but survives for long times and saturates to a value at long times. The Hall response survives for infinitly long times. Similarly, Fig. 4.6 shows the Hall current in different phases has different magnitudes for fixed momentum but overall behavior is same. The inset in Fig.4.6 shows that Hall current survives for long times.

Now we want to calculate current due to the whole valence band, which is

$$J_{Total} = \int_0^\infty \frac{J_{Hall}kdk}{2\pi}.$$

In order to facilitate numerical calculation, we have obtained results which are valid in the long time limit by replacing the Bessel function $\mathbf{J_1[X]}$ by $Cos[\pi/4 + X]$. The numerical results are plotted in Fig. 4.7. This shows that current is decaying but is non zero for long times (inset of Fig.4.7).

4.4 Results

We find that Hall current is oscillatory when the system is either in the insulating or the nodal phase and has a beating pattern when plotted for different times. For $t_2 \to \infty$ we are left with the last term in Eq.4.12 which is function of t_1. This term when numerically integrated shows Hall current which is purely dependent on time t_1, as seen in Fig.4.8. This figure also shows that if the time t_1 at which the pulse acts is very long then the reminant Hall current dies off.

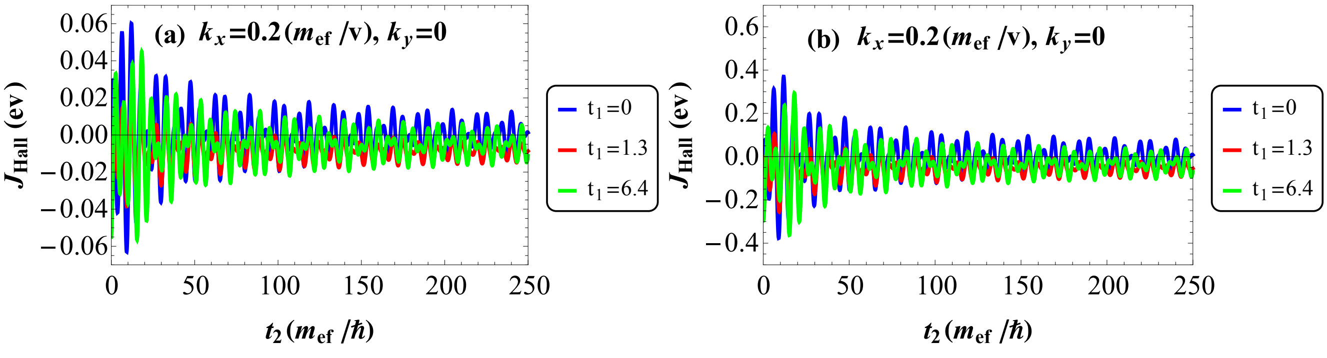

$(\mathbf{a})\boldsymbol{\Delta_0} < \frac{\mathbf{e^2A_0^2}}{\mathbf{2m^*}}$ $(\mathbf{b})\boldsymbol{\Delta_0} = \frac{\mathbf{e^2A_0^2}}{\mathbf{2m^*}}$

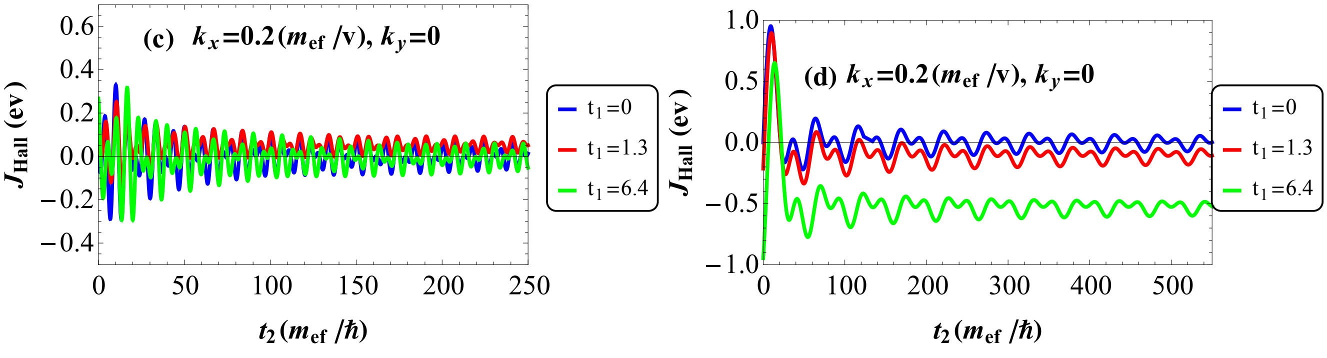

$(\mathbf{c})\boldsymbol{\Delta_0} > \frac{\mathbf{e^2A_0^2}}{\mathbf{2m^*}}$ $(\mathbf{d})\boldsymbol{\Delta_0} = \mathbf{0}$

Figure 4.5: Current response of a ring of states taking $eA = 0.3\mathring{A}^{-1}$, $eA_0 = 0.01\mathring{A}^{-1}$.

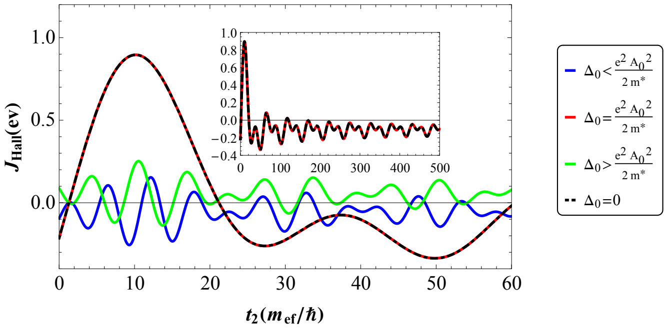

$k_x = 0.2(m_{ef}/v), k_y = 0$

Figure 4.6: Current response of ring of states taking $eA = 0.3\mathring{A}^{-1}$, $eA_0 = 0.01\mathring{A}^{-1}$ and $t_1 = 1.3\frac{m_{ef}}{\hbar}$. The inset shows $\Delta_0 = \frac{e^2A_0^2}{2m^*}$ and $\Delta_0 = 0$ case for very long times.

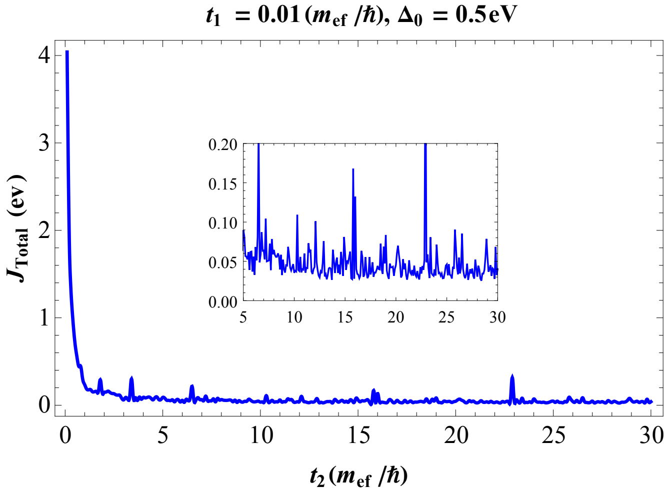

Figure 4.7: Current response of the valence band taking $eA = 0.3\mathring{A}^{-1}$ and $eA_0 = 0.01\mathring{A}^{-1}$. The inset shows the magnified view of J_{Total} in the specific t_2 range.

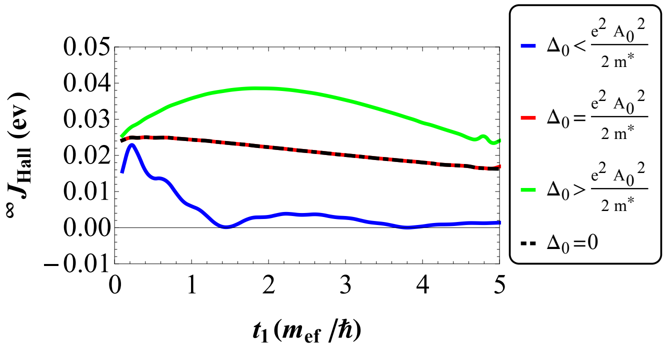

Figure 4.8: Current response of the valence band for $t_2 \to \infty$ taking $eA = 0.3\mathring{A}^{-1}$ and $eA_0 = 0.01\mathring{A}^{-1}$

.

Chapter 5

Summary

We have shown in Ch.(2) that Berry curvature is non-zero and opposite for both valleys in silicene when placed in proximity with ferromagnetic material and exposed to perpendicular electric and magnetic fields. The contrasting orbital magnetic moment for both valleys couple the valley degree of freedom with the magnetic field. This gives the energy splitting in the presence of a magnetic field. Proximity effect shifts the maxima of magnetic moment. It is interesting to notice that magnetic moment rely strictly on the valley degree of freedom, which is similar to the properties of spin and a Zeeman like interaction appears. This behavior leads to valley-spin locking. Moreover, this magnetic moment can be tuned by an external electric field and exchange term. Valley polarization of electrons and Hall conductivities that are experimentally detectable quantities were also discussed in Ch.(2). We find signatures of a quantum phase transition from a topological insulator to a band insulator phase in both the valley and spin Hall conductivities. Our work shows that the role of pseudospin is very important for silicene as both valleys have opposite behaviors in the applied fields. When an external magnetic field is switched off but breaking the TRS through proximity effect, the system allows single spin and valley to transport, thus a perfect spin and valley half metal can be constructed which can be useful in real devices[96].

A study of magnetic susceptibility of Weyl semimetals in a tilted magnetic field was presented in Ch.(3). We have shown that all the three components of susceptibility for topological semimetals are non-zero and exhibit unique characteristics that depend on Fermi energy, orientation and strength of magnetic field. As the susceptibility depends on the magnetic field orientation, this shows that Weyl semimetals have anisotropic magnetic response[145]. Spin susceptibility is shown to depend linearly on Fermi energy. For $T \to 0$, spin-orbit susceptibility is an even function of Fermi energy and orbital susceptibility has singular and strongly diamagnetic behavior when the Fermi level is at the charge neutrality point. The total magnetic susceptibility shows that the spin susceptibility is a weaker phenomenon as compared to orbital and spin-orbit susceptibility because of the smaller magnitude of Zeeman term. It can be seen that around the nodes, the strong diverging behavior of orbital susceptibility dominates. We also show that the orbital and the spin-orbit contribution to susceptibility arises entirely from the $n = 0$ LLs. Interestingly, we find that both spin-orbit and orbital contribution to susceptibility can be tuned by the orientation of the magnetic field; they can be made to vanish from a finite value by changing the orientation of the magnetic field. Spin-orbit susceptibility goes from finite value to zero with change in orientation of magnetic field. Whereas orbital susceptibility goes from zero to finite value when conduction band is approached. This dependence of susceptibilities on orientation of magnetic field helps us to separate the magnetic response arising from spin and orbital coupling with magnetic field. In order to separately observe the spin and orbital response predicted in this study, x-ray magnetic circular dichroism technique can possibly be employed[146].

In Ch.(4) of the thesis, non equilibrium Hall response of semi-Dirac materials was studied. This required preparing the system in non equilibrium states through a quantum quench protocol. We show that in the non equilibrium setting, there is non-zero Hall response even when instantaneous TRS is present and the Hall current persists for long times. This is in contrast to the equilibrium case where the system is required to break TRS for a Hall response.

This is worth mentioning here that for future study classifications and making of periodic tables of topological insulators and topological semimetals is an open area of study. Response of the materials to external fields can make classification easy.

Bibliography

[1] K. V. Klitzing, G. Dorda and M. Pepper, Phys. Rev. Lett. 45 494 (1980).

[2] D. J. Thouless, M. Kohmoto,M. P. Nightingale, and M. den Nijs, Phys. Rev. Lett. 49, 405(1982).

[3] R.B. Laughlin, Phys. Rev. B 23, 5632 (1981).

[4] D. J .Thouless, M. Kohomoto, M. P. Nightangale and M.den Nijs, Phys. Rev. Lett. 49, 405 (1982).

[5] Q. Niu; D. J. Thouless,and Y. S. Wu, Phys. Rev. B 31, 3372 (1985).

[6] M. Kohomoto, annals of physics 160, 343 (1985).

[7] B. I. Halperin, Phys. Rev. B 25, 2185 (1982).

[8] X. G. Wen, Adv. Phys. 44, 405 (1995).

[9] M.Z. Hasan, and C.L. Kane, Rev. Mod. Phys. 82, 3045 (2010).

[10] X-L Qi and S-C Zhang, Rev. Mod. Phys. 83, 1057 (2011).

[11] C. L. Kane and E. J. Mele, Phys. Rev. Lett. 95, 146802 (2005).

[12] C. L. Kane, and E. J. Mele, Phys. Rev. Lett. 95 226801(2005).

[13] L. Fu, C. L. Kane, and E. J. Mele, Phys. Rev. Lett. 98, 106803 (2007).

[14] J. E. Moore and L. Balents, Phys. Rev. B 75, 121306(R) (2007).

[15] R. Roy, Phys. Rev. B 79, 195322 (2009).

[16] Y. Xia et.al., Nature Physics 5, 398 (2009).

[17] H. Zhang, C-X. Liu, X-L. Qi, X. Dai, Z. Fang and S-C Zhang, Nature Physics, 5 438 (2009).

[18] A. A. Burkov, M. D. Hook and Leon Balents, Phys. Rev. B 84, 235126 (2011).

[19] X. Wan, A. M. Turner, A. Vishwanath, and S. Y. Savraso, Phys. Rev. B 83, 205101 (2011).

[20] S. M. Young, S. Zaheer, J. C. Y. Teo, C. L. Kane, E. J. Mele, and A. M. Rappe, Phys. Rev. Lett. 108, 140405 (2012).

[21] S. Murakami, New J. Phys. 9, 356 (2007).

[22] Z.Wang, Y. Sun, X.-Q. Chen, C. Franchini, G. Xu, H.Weng, X. Dai, and Z. Fang, Phys. Rev. B 85, 195320 (2012).

[23] T. O. Wehling, A. M. Black-Schaffer, and A. V. Balatsky, Adv. Phys. 63, 1 (2014)

[24] O. Vafek and A. Vishwanath, Annu. Rev. Condens. Matter Phys. 5, 1 (2014).

[25] S. D. Sarma, S. Adam, E.H. Hwang and E. Rossi, Rev. Mod. Phys. 83, 407 (2011).

[26] B. Fu, H-W Wang, S-Q Shen, Phys. Rev. B 101, 12503 (2020).

[27] J. C. Sandoval-Santana, V. G. Ibarra-Sierra, A. Kunold, G. G. Naumis, J. Appl. Phys. 127, 234301 (2020).

[28] A. L. Phan, D. N. Le, V. H. Le, P. Roy, Physica E 121, 114084 (2020).

[29] Y. D. Lensky, J. C. W. Song, P. Samutpraphoot, and L. S. Levitov, Phys. Rev. Lett. 114, 256601 (2015).

[30] M. Trescher, B. Sbierski, P. W. Brouwer, and E. J. Bergholtz, Phys. Rev. B 91, 115135 (2015).

[31] D. F. Perepichka and F. Rosei, Small 2 22 (2005).

[32] G. G. Guzmn-Verri, L. C. Lew Yan Voon, Phys. Rev. B 76 075131 (2007).

[33] P. De Padova, C. Quaresima, C. Ottaviani, P. M. Sheverdyaeva, P. Moras, C. Carbone, D. Topwal, B. Olivieri, A.R. Kara, H. Oughaddou, B. Aufray, and G. L. Lay, App.Phys. Lett. 96 261905 (2010).

[34] P. De Padova, C. Quaresima, B. Olivieri, P. Perfetti, and G. L. Lay, App.Phys. Lett. 98 081909 (2011).

[35] Fleurence, R. Friedlein, T. Ozaki, H. Kawai, Y. Wang, and Y. Yamada-Takamura, Phys. Rev. Lett. 108 245501 (2012).

[36] L. Tao, E. Cinquanta, D. Chiappe, C. Grazianetti, M. Fanciulli, M. Dubey, A. Molle and D. Akinwande, Nature Nanotechnology 10 227 (2015).

[37] R. Pawlak, C. Drechsel, P. D'Astolfo, M. Kisiel, E. Meyer and J. I. Cerda, pnas, 117 228 (2020).

[38] C. Liu, W. Feng, and Y. Yao, Phys. Rev. Lett. 107 076802 (2011).

[39] N. D. Drummond, V. Zolyomi, and V. I. Fal'ko, Phys. Rev. B 85 075423 (2012).

[40] T. Aftab, Physics Letters A 381 953 (2017).

[41] D. A. Osborne, T. Morishita, S. A. Tawfik, T. Yayama and M. J. S. Spencer, Phys. Chem. Chem. Phys. 21, 17521 (2019).

[42] L. Razavi, H. Raissi, H. Hashemzadeh, F. Farzad, J Biomol Struct Dyn. 0, 1 (2020).

[43] T. Tarun, D. K. K. Randhawa, P. Singh, B. C. Choudhary, G. K. Walia and N. Kaur, J. of Molecular Modeling 26, 63 (2020).

[44] S. Alesheikh, N. Shahtahmassebi, M. R. Roknabadi, R. P. Shahri, Phys. Lett. A 382, 595 (2018).

[45] L.B. Drissi, H. Ouarrad, F. Z. Ramadan, and W. Fritzsche, RSC. Adv. 10, 801 (2020).

[46] T. Aftab, K. Sabeeh, Journal of Applied Physics 127, 163905 (2020).

[47] S.-Y. Xu, I. Belopolski, N. Alidoust, M. Neupane, G. Bian, C. Zhang, R. Sankar, G. Chang, Z. Yuan, C.C. Lee et al., Science 349, 613 (2015).

[48] G. Xu, H. Weng, Z. Wang, Xi Dai, and Z. Fang, Phys. Rev. Lett. 107, 186806 (2011).

[49] S.-M. Huang, S.-Y. Xu, I. Belopolski, C. C. Lee, G. Chang, B. Wang, N. Alidoust, G. Bian, M. Neupane, C. Zhang et al., Nat. Commun. 6, 7373 (2015).

[50] B. Lv, H.Weng, B. Fu, X.Wang, H. Miao, J.Ma, P. Richard, X. Huang, L. Zhao, G. Chen et al., Phys. Rev. X 5, 031013 (2015).

[51] A. A. Burkov and Leon Balents, Phys. Rev. Lett. 107, 127205 (2011).

[52] H. Weng, C. Fang, Z. Fang, B. A. Bernevig, and X. Dai, Phys. Rev. X 5, 011029 (2015).

[53] S.Y. Xu, C. Liu, S. K. Kushwaha, R. Sankar, J. W. Krizan, I. Belopolski, M. Neupane, G. Bian, N. Alidoust, T.R. Chang et al., Science 347, 294 (2015).

[54] S. Borisenko, Q. Gibson, D. Evtushinsky, V. Zabolotnyy, B. Buchner, and R. J. Cava, Phys. Rev. Lett. 113, 027603 (2014).

[55] Z. K. Liu, B. Zhou, Y. Zhang, Z. J. Wang, H. M. Weng, D. Prabhakaran, S.K.Mo, Z. X. Shen, Z. Fang, X. Dai, Z. Hussain, and Y. L. Chen, Science 343, 864 (2014).

[56] M. Brahlek, N. Bansal, N. Koirala, S.Y. Xu, M. Neupane, C. Liu, M. Z. Hasan, and S. Oh, Phys. Rev. Lett. 109, 186403 (2012).

[57] J. C. Budich and M. Heyl, Phys. Rev. B 93, 085416 (2016).

[58] M. D. Caio, N. R. Cooper, and M. J. Bhaseen, Phys. Rev. Lett. 115, 236403 (2015).

[59] H. Dehghani, T. Oka, and A. Mitra, Phys. Rev. B 91, 155422 (2015).

[60] A. G. Grushin, S. Roy, M. Haque, J. Stat. Mech.:Theory Exp. 2016, 083103 (2016).

[61] P. Hauke, M. Lewenstein, and A. Eckardt, Phys. Rev. Lett. 113, 045303 (2014).

[62] M. Killi, S. Trotzky, A. Paramekanti, Phys. Rev. A 86, 063632 (2012).

[63] M. Greiner, O. Mandel, T.W. Hansch, and I. Bloch, Nature (London) 419, 51 (2002).

[64] T. Oka and H. Aoki, Photovoltaic Hall effect in graphene, Phys. Rev. B 79, 081406(R) (2009).

[65] T. Kitagawa, T. Oka, A. Brataas, L. Fu, and E. Demler, Phys. Rev. B 84, 235108 (2011).

[66] L. D. Alessio and M. Rigol, Nat. Commun. 6, 8336 (2015).

[67] M. S. Rudner, N. H. Lindner, E. Berg, and M. Levin, Phys. Rev. X 3, 031005 (2013).

[68] L. E F Foa Torres, P. M. Perez-Piskunow, C. A. Balseiro, and G. Usaj, Phys. Rev. Lett. 113, 266801 (2014).

[69] T. Aftab and K. Sabeeh, Far from equilibrium Dynamical Response in Photoinduced Semi-Dirac Materials, in preparation

[70] D. Xiao, M.C. Chang, Q. Niu, Rev. Mod. Phys. 82 1959 (2010).

[71] D. Xiao, W. Yao, and Q. Niu, Phys. Rev. Lett. 99 236809 (2007).

[72] W. Yao, D. Xiao, and Q. Niu, Phys. Rev. B 77 235406 (2008).

[73] M. Tahir, A. Manchon, K. Sabeeh and U. Schwingenschlogl, Appl. Phys. Lett. 102 162412 (2013).

[74] M. Tahir and U. Schwingenschlogl, Scientific Reports 3 1075 (2013).

[75] D. Xiao, G.B. Liu, W. Feng, X. Xu and W. Yao, Phys. Rev. Lett. 108 196802 (2012).

[76] T. Cai, S. A. Yang, X. Li, F. Zhang, J. Shi, W. Yao and Q. Niu, Phys. Rev. B 88 115140 (2013).

[77] B. V Duppen, P. Vasilopoulos and F. M. Peeters, Phys. Rev. B 90 035142 (2014).

[78] Z. Yu, H. Pan and Y. Yao, Phys. Rev. B 92 155419 (2015).

[79] Y. Hajati and Z. Rashidian, Microstructures 92 264 (2016).

[80] Y. Shimazaki, M. Yamamoto, I. V. Borzenets, K. Watanabe, T. Taniguchi and S. Tarucha, Nature Physics 11 1032 (2015).

[81] J. Zhao , H. Liu, Z. Yu , R. Quhe, S. Zhou , Y. Wang, C. C. Liu, H. Zhong , N. Han, J. Lu, Y. Yao, K.Wu, Science 83 24 (2016).

[82] J. Kim, X. Hong, C Jin, S-F Shi, C-Yuan, S. Chang, M-H Chiu, L-Jong Li and F. Wang, Science, 346 1205 (2014).

[83] Y. J.Zhang, T. Oka, R. Suzuki, J. T. Ye and Y. Iwasa, Science 344 725 (2014).

[84] Q. H.Wang, K.Kalantar-Zadeh, A.Kis, J. N. Coleman and M. S.Strano, Nature Nanotechnology 7 699 (2012).

[85] A.Rycerz, J. Tworzyd and C. W. J. Beenakker, Nature Physics 3 172 (2007) .

[86] J. TworzydĊo, I. Snyman, A. R. Akhmerov, and C. W. J. Beenakker, Phys. Rev. B 76 035411 (2007).

[87] R. Akhmerov and C. W. J. Beenakker, Phys. Rev. Lett. 98 157003 (2007).

[88] M. Yang, R. Q. Wang and Y. K. Bai, Physics Letters A 379 1732 (2015).

[89] C. E Nebel, Nature materials, 12 690 (2013).

[90] M. Ezawa, J. Phys. Soc. Jpn. 81 064705 (2012).

[91] H. Pan, Z. Li, C.C. Liu, G. Zhu, Z. Qiao and Y. Yao, Phys. Rev. Lett 112 106802 (2014).

[92] M. Ezawa, New J. Phys 14 033003 (2012).

[93] H. Pan, Z. Li, C.C.Liu, G. Zhu, Z. Qiao and Y. Yao, Phys. Rev. Lett 112, 106802 (2014).

[94] C. J. Tabert and E. J. Nicol, Phys. Rev. Lett. 110, 197402 (2013).

[95] X. J. Qiu, Y. F. Cheng, Z. Z. Cao and J. M. Lei, Appl. Phys. 48, 465105 (2015).

[96] W. Sa-Ke, W. Jun, Chin. Phys. B 24, 037202 (2015).

[97] C. Liu, W. Feng, and Y. Yao, Phys. Rev. Lett. 107, 076802 (2011).

[98] N. D. Drummond, V. Zolyomi, and V. I. Fal'ko, Phys. Rev. B 85, 075423 (2012).

[99] C-C Liu, H. Jiang and Y. Yao, Phys. Rev. B 84, 195430 (2011).

[100] Z. Song, R. Quhe, S. Liu, Y. Li, J. Feng, Y. Yang, J. Lu and J. Yang, Scientific Reports 5, 13906 (2015).

[101] D. Xiao, J. Shi and Q. Niu, Phys. Rev. Lett. 95, 137204 (2005).

[102] B. Q. Lv et al, Phys. Rev. X 5, 031013 (2015).

[103] B. Q. Lv et al., Nat. Phys 11, 9 (2015).

[104] V. Aji, Phys. Rev. B 85, 241101(R) (2012).

[105] A. A. Zyuzin and A. A. Burkov, Phys. Rev. B 86, 115133 (2012).

[106] M. M. Vazifeh and M. Franz, Phys. Rev. Lett. 111, 027201 (2013).

[107] D. T. Son and B. Z. Spivak;,Phys. Rev. B 88, 104412 (2013).

[108] C-X Liu, P. Ye, and X-L. Qi, Phys. Rev. B 92, 119904(E) (2015).

[109] A.A. Burkov, Phys. Rev. Lett. 113, 247203 (2014).

[110] M. Alidoust, Phys. Rev. B 98, 245418 (2018).

[111] B. Rosenstein, B. Ya. Shapiro, Dingping Li, and I. Shapiro, Phys. Rev. B 97, 144510 (2018).

[112] M. Koshino and I. F. Hizbullah, Phys. Rev. B 93, 045201 (2016).

[113] J. W. McClure, Phys. Rev. 104, 666 (1956).

[114] A. Mogulkoc, M. Modarresi and A.N. Rudenko, Phys. Rev. B 96, 085434 (2017).

[115] A. A. Zyuzin, M. D. Hook, and A. A. Burkov, Phys. Rev. B 83, 245428 (2011).

[116] S. S. Pershoguba, D. S. L. Abergel, Victor M. Yakovenko, and A. V. Balatsky, Phys. Rev. B 91, 085418 (2015).

[117] A. A. Zyuzin and A. A. Burkov, Phys. Rev. B 83, 195413 (2011).

[118] Y. Ominato, S. Tatsumi, and K. Nomura, Phys. Rev. B 99, 085205 (2019).

[119] V. Pardo and W. E. Pickett, Phys. Rev. Lett. 102, 166803 (2009).

[120] V. Pardo and W. E. Pickett, Phys. Rev. B 81 ,035111 (2010).

[121] V. Damljanovic, R. Gajic, Journal of Physics. Condensed Matter: an Institute of Physics Journal 29, 185503 (2017).

[122] S. Katayama, A. Kobayashi, and Y. Suzumura, J. Phys. Soc. Jpn. 75, 054705 (2006).

[123] Y. Hasegawa, R. Konno, H. Nakano and M. Kohomoto, Phys. Rev. B 74, 033413 (2006).

[124] O. Bahat-Treidel, O. Peleg, M. Grobman, N. Shapira, M. Segev, and T. Pereg-Barnea, Phys. Rev. Lett. 104, 063901 (2010).

[125] L. Tarruell, D. Greif, T. Dehlinger, and T. Easlinger, Nature (London) 483, 302 (2012).

[126] F. PiİIchon, J. N. Fuchs, A. Raoux, and G. Montambaux, J. Phys.: Conf. Ser. 603, 012001 (2015).

[127] S. Banerjee, R. R. P. Singh, V. Pardo, and W. E. Pickett, Phys. Rev. Lett. 103 ,016402 (2009).

[128] S. Banerjee, and W. E. Pickett, Phys. Rev. B 86 ,075124 (2012).

[129] P. Delplace, A. Gomez-Leon, and G. Platero, Phys. Rev. B 88, 245422 (2013).

[130] P. Adroguer, D. Carpentier, G. Montambaux, and E. Orignac, Phys. Rev. B 93, 125113 (2016).

[131] M. Sanderson, S. Huang, Y. Zhang, and C. Zhang, J. Phys. D: Appl. Phys. 51, 205302 (2018).

[132] J. P. Carbotte, K. R. Bryenton, and E. J. Nicol, Phys. Rev. B 99, 115406 (2019).

[133] M. Oliva-Leyva and G. G. Naumis, Phys. Rev. B 93, 035439 (2016).

[134] P. K. Pyatkovskiy and T. Chakraborty, Phys. Rev. B 93, 085145 (2016).

[135] K. Saha, R. Nandkishore, and S. A. Parameswaran, Phys. Rev. B 96, 045424 (2017).

[136] K. Ziegler and A. Sinner, Europhys. Lett. 119, 27001 (2017).

[137] P. Nualpijit, A. Sinner, and K. Ziegler, Phys. Rev. B 97, 235411 (2018).

[138] H. Huang, Z. Liu, H. Zhang, W. Duan, and D. Vanderbilt, Phys. Rev. B 92, 161115 (2015).

[139] J.H. Wilson, J. C. W. Song and G. Refael, Phys. Rev. Lett. 117, 235302 (2016)

[140] S. Will, D. Iyer and M. Rigol, Nat. Commun. 6, 6009 (2015).

[141] B. K. Stuhl, H. I. Lu, L. M. Aycock, D. Genkina, and I. B. Spielman, Science 349, 1514 (2015).

[142] M. Atala, M. Aidelsburger, J. T. Barreiro, D. Abanin, T. Kitagawa, E. Demler, and I. Bloch, Nat. Phys. 9, 795 (2013).

[143] G. Jotzu, M. Messer, R. Desbuquois, M. Lebrat, T. Uehlinger, D. Greif, and T. Esslinger, Nature (London) 515, 237 (2014).

[144] K. Saha, Phys. Rev. B 96, 081103(R) (2016).

[145] K. Halterman, M. Alidoust, and A. Zyuzin, Phys. Rev. B 98, 085109 (2018).

[146] T. Ueno, J. Sinha, N. Inami, Y. Takeichi, S. Mitani, K. Ono and M. Hayashi, Scientific Reports 5, 14858 (2015).